Sea level anomalies using altimetry, model and tide gauges along the African coasts in the Eastern Tropical Atlantic Ocean: inter-comparison and temporal variability

Habib B Dieng, Isabelle Dadou, Fabien Léger, Yves Morel, Julien Jouanno, Florent Lyard, Damien Allain

Sea level anomalies using altimetry, model and tide gauges along the African coasts in the Eastern Tropical Atlantic Ocean: inter-comparison and temporal variability

Habib B. Dieng[1], Isabelle Dadou[1], Fabien Léger[1], Julien Jouanno[1], Yves Morel[1], Florent Lyard[1] and Damien Allain[1]

1. LEGOS: CNRS/CNES/IRD/UT3-PS, 14 Avenue E. Belin, 31400 Toulouse cedex, France

Revised version : Advances in Space Research

August 2019

Abstract

Because of sparse in situ measurements, the use of altimeter and ocean models are currently the only options to understand the coastal variability of sea level anomalies (SLA) near the African coasts of the Eastern Tropical Atlantic Ocean (ETAO: 35°S–25°N; 25°W–African coasts). In this study, three SLA products derived from altimetry (X-TRACK and CMEMS) and from a regional ocean model (NEMO) are validated near the coast using the 14 tide gauges (TGs) available in the region. Statistical analysis (correlation, standard deviation and root mean square) are performed to compare our three products with the TG. We then analyze the sub-seasonal to inter-annual variability of SLAs (i.e. from 20 days up to 2 years) over the period January 2008 – December 2014.

We found a very good agreement between altimetry, model and TGs near the coasts of Senegal (10°N – 25°N) and Gulf of Guinea (10°S – 10°N). This is not the case near the coast of Benguela (south of 10°S) and is mainly explained by the combined effects of the position of TGs (located in semi-enclosed bays), the geophysical corrections used in the computations of the SLA derived from altimetry (i.e. tide, dynamical atmospheric correction -DAC- and sea state bias -SSB-). In addition, the low spatial resolution of the CMEMS and model data do not allow a good description of the small scale oceanic and atmospheric variability, which dominates in the Benguela upwelling system.

We then show, with all products, that the temporal variability of SLA is mainly seasonal (annual and semi-annual) throughout the ETAO region. The altimetry data also show some inter-annual (15 to 24 months) variability in the equatorial band, which can be related to equatorial Kelvin waves. This is less pronounced with the NEMO model and does not appear over the whole equatorial band.

We show that high spatial resolution and improved altimetric geophysical corrections near the coast can each reduce near-shore data errors by up to 10%. However, despite these improvements, agreements between SLA products are still unsatisfactory in the Benguela region, suggesting that efforts need to be intensified on geophysical corrections and in increasing the temporal and spatial resolution of data near the coast. Moreover, there exist gaps in TG measurements, along the West African coast, especially in the Benguela region. The TG network should thus be completed.

1. Introduction

The monitoring of the African coastal area represents a major societal challenge, from short term economic issues (fishery is mostly artisanal) to risk assessment associated with climate change (e.g. sea level rise). The equilibrium and high to low frequency variability of the dynamics and of biogeochemical or ecological systems of this region is controlled by coastal processes (river plumes, tides, topographic waves), atmospheric forcing (precipitations, transient or permanent coastal upwelling/downwelling currents, steric effects associated with warming) and exchange with the deep ocean. Sea-level observations represent a major source of information to monitor the ocean evolution at different scales. For several centuries, tide gauges (TG) have permitted to follow the sea level variations near the coast. Since 1993 sea level is routinely measured using high-precision altimetric satellite (e.g. Topex/Poseidon, Jason-1/2/3, Envisat). While altimetry from space has enabled us to highlight the regional variability of sea level and meso-scale dynamics in the open ocean, it still provides incomplete information in coastal areas in the first 50 km from the coasts, especially in the first 15 km due to the perturbation of radar echoes by the continents (Cipollini et al., 2017). In recent years, efforts have been made to improve altimetric data in coastal areas (Vignudelli et al., 2011), using *(1)* new altimeter instrument (Veron et al., 2015), *(2)* new editing and post-processing techniques dedicated to coastal zone (Birol et al., 2017) and *(3)* new retracking methods using empirical models adapted to take into account non-standard radar waveform (Passaro et al., 2017). In addition, high resolution models also allow us to study regional and coastal variability of sea level. Before being used in specific areas, these new altimetry and model datasets have to be validated, in particular in the coastal region using in-situ data. Given the potentially strong biases, validation is now more focused in the coastal zone using TGs. This has been done mostly along coasts of America (e.g. Salazar-Ceciliano et al., 2018; Risien and Strub, 2016; Ruiz-Etcheverry et al., 2015; Tseng et al., 2014), Western Europe (e.g. Fenoglio-Marc et al., 2015; Gómez-Enri et al., 2016 and 2018; Vu et al., 2018; Gonzalez et al., 2019), Mediterranean sea (e.g. Bonnefond et al., 2015; Jebri et al., 2016; Marijan et al., 2017; Birol et al., 2017), Asia and Australia (e.g. Liu and Huang 2019; Peng and Deng, 2018; Kumar et al., 2017; Idris et al., 2017), where there are high quality TGs, covering the entire altimetry period and equipped with GPS to correct the effect of local vertical ground motions (Simon et al., 2013; Le Cozannet et al., 2015; Melet et al., 2016). Only few sea level anomalies (SLA) validation studies have been conducted along the coast of the Eastern Tropical Atlantic Ocean (ETAO: 35°S – 25°N; 25°W – African coasts). Moreover these

previous studies cover a very small area and usually only use a single TG (e.g. Verstraete and Park, 1995; Rubio et al., 2009; Melet et al., 2016; Angnuureng et al., 2018). Thus, the SLA signals associated with coastal processes remains little studied in the ETAO region, even though this region encompasses many specific and interesting dynamics: large-scale zonal equatorial currents and waves (Kelvin, Rossby, Tropical Instability Waves), strong coastal currents, equatorial and coastal trapped waves as well as internal tides (Cipollini et al., 1998; Djakouré et al., 2014 and 2017; Bachèlery et al., 2016; Herbert et al., 2016; Baquet, 2018), the presence of both equatorial and coastal upwelling cells, gyre structures such as the Guinea and Angola domes (e.g. Schott et al., 2004; Doi et al., 2009; Doi et al., 2010). The ETAO has been also identified as one of the key oceanic regions to improve climate simulations as there exist persistent warm biases in climate global models in this region (e.g. Richter et al., 2014). Indeed, the equatorial region is a major contributor for ocean/atmosphere heat and water fluxes.

Despite these challenges, there are few in-situ measurements in this area. Only 14 TGs are available (against more than a hundred in other regions of the globe) for the validation of altimetry data and the time period covered by these data remains sparse and does not even cover the entire altimetry period. The existing TG data are thus precious and it is now essential to use them to validate altimetric data, a prerequisite to study SLA variability in this region, and for instance estimate the meso-scale activities near the coast in the ETAO.

In the present study, the main objective is to validate the SLA data in the coastal area of the ETAO region. We used both along track observations (using the X-TRACK data provided by the CTOH, Birol et al., 2017, see section 2.1.1) and gridded product (CMEMS altimetry data provided by Copernicus Marine Service, Pujol et al., 2016 and Taburet et al., 2019, see section 2.1.2). Satellite altimetry data will be confronted to results from realistic numerical simulations of the ETAO region (Jouanno et al., 2011 and 2017; see section 2.2) and available TG data between January 2008 and December 2014 (see section 2.3), analyzing sub-seasonal (> 20 days) to inter-annual variability (<2 years). We limit our investigations to inter-annual signals less than 2 years because the time period of the TG data is limited to 2008 – 2014, representing only 7 years. Validation is based on the comparison with standard statistical metrics (correlation, standard deviation and RMS -root mean square-) and the direct comparison of temporal variability of SLA signals for each dataset, for periods between 20 days and 2 years. To better study this vast area, we considered three sub-regions having different spatial and temporal variability (e.g. Brandt et al., 2010; Lee et al., 2012; Djakouré et

al., 2014, 2016; Ndoye et al., 2017): Senegal (10°N – 25°N), Gulf of Guinea (10°S – 10°N) and Benguela (south of 10°S). We also study the impact of improvements of the altimetric geophysical corrections by comparing two versions of the CMEMS product, as well as the impact of the model spatial resolution using the NEMO model with two different spatial resolutions (1/4° and 1/12 °).

2. Sea level data and Method

2.1 Altimetry data

For the altimeter-based sea level data, we use two different products: *(1)* X-TRACK the along track data from « Centre de Topographie des Océans et de l'Hydrosphère » (CTOH) and *(2)* the gridded data from Copernicus Marine Environment Monitoring Service (CMEMS).

The sea surface height (*SSH*) for both products is calculated by the following relation (Pujol et al., 2016, Birol et al., 2017 and Taburet et al., 2019):

$$SSH = H - (R + Environmental\_corrections + Geophysical\_corrections) \quad (1)$$

where *H* is the altitude of the center of mass of the satellite relative to the reference ellipsoid. H is estimated using precise orbit determination technique. *R* is the nadir altimeter range which is the distance from the mass center of the satellite to the sea surface, taking into account instrumental corrections. *Environmental_corrections* is the sum of the corrections of electromagnetic wave propagation of the altimeter radar in the inhomogeneous atmosphere and is given by the equation:

$$Environmental\_corrections = dry\_tropo\_corr + wet\_tropo\_corr + iono\_corr \quad (2)$$

where *dry_tropo_corr*, *wet_tropo_corr* and *iono_corr* are calculated taking into account the observed state of the dry troposphere, wet troposphere and ionosphere crossed by the radar electromagnetic waves.

Geophysical_corrections is given by the equation:

$$Geophysical\_corrections = solidEarth\_tide + pole\_tide + load\_tide + SSB + ocean\_tide + DAC \quad (3)$$

where *solidEarth_tide*, *pole_tide*, *load_tide*, *SSB*, *ocean_tide* and *DAC* are the corrections of solid Earth tide, pole tide, loading tide, sea state bias, ocean tide and dynamical atmospheric, respectively. The sum of ocean tide and loading tide is the elastic ocean tide.

2.1.1 X-TRACK: a coastal along track sea level product

X-TRACK provides along-track sea level data for the coastal zones. X-TRACK data cover the period 1993 – 2016 in the ETAO region. This product (level 3; version: DOI 10.6096/CTOH_X-TRACK_2017_01) is provided by the CTOH (http://ctoh.legos.obs-mip.fr/) and is based on the combination of data from Topex/Poseidon, Jason-1 and Jason-2/OSTM (Ocean Surface Topography Mission) missions. Using the 1 Hz Geophysical Data Record (GDR) along-track data for each of the three altimetric missions, the CTOH applies altimeter corrections based on an editing method: starting with the selection of valid ocean data and a precise land-mask, the altimeter measurements and the geophysical and environmental correction terms (except the *solidEarth_tide* and *load_tide* terms) are carefully analyzed. The characteristics of each corrective term are edited along-track and statistical outliers are detected and removed. To compensate for the missing data corrections (outliers), interpolation or extrapolation methods are applied, using the valid data to reconstruct each discarded correction. After the editing method, the X-TRACK software (Birol et al., 2017) provides an along track *SSH* at 1Hz along the selected track with a spatial resolution of 6 to 7 km. The inter-track gap is about 300 km at the equator. Details on X-TRACK data processing for the version used in the present paper can be found in Birol et al. (2017). X-TRACK increases the altimetry data accuracy over coastal areas and gives more information on sea level variation related to the ocean dynamics at the coast.

The last two terms of the geophysical corrections (*ocean_tide* and *DAC*), important in coastal areas, are calculated using the global tide model FES2012 (Finite Element Solution 2012, see Carrère et al., 2012) and the combination of high-frequency elevations from the global Mog2D/T-UGOm 2D model (Carrère and Lyard, 2003) and Inverse Barometer (IB) model (Wunsch and Stammer, 1997).

FES2012 is based on the spectral barotropic tidal model T-UGOm (Carrère et al., 2012). FES2012 assimilates Topex/Poseidon, Jason-1, Jason-2/OSTM, ERS-1, ERS-2 and Envisat altimeter data to correct the model tide. It provides data on regular grids of 1/16° resolution.

MOG2D-G/T-UGOm is a high resolution nonlinear barotropic model, with unstructured grid, forced with the European Center for Medium-range Weather Forecasting (ECMWF) pressure and wind fields (with a temporal resolution of 6 hours). IB model provides the inverse barometer correction, assuming a static response from the ocean to atmospheric pressure forcing. IB fields are available with a spatial resolution of 1/4°.

2.1.2 CMEMS gridded data

The CMEMS sea level products are dedicated to the study of meso-scale activity with the best estimate and sampling of the ocean. In addition, a lot of efforts have been made to improve data near the coast. For the present study, we tested two gridded data versions from Copernicus Marine Environment Monitoring Service (CMEMS, http://marine.copernicus.eu/), available over the periods 1993–2017 (CMEMS/DT2014, see Pujol et al., 2016) and 1993–2018 (CMEMS/DT2018, see Taburet et al., 2019). The gridded data (level 4) are based on a larger set of altimetry missions (repeated track, geodetic and new interleaved orbits) merged together: data of reference missions (Topex/Poseidon, Jason-1, Jason-2/OSTM and Jason-3), complementary missions (ERS-1, ERS-2, ENVISAT, Saral/AltiKa and Sentinel-3A) and opportunity missions (Geosat follow-on -GFO-, CRYOSAT-2 and HY-2A) are used. Data are then cross validated, filtered from residual noise and small scale signals, sub-sampled, and an optimal interpolation is finally applied on the along-track data to compute 2D-gridded sea level (Pujol et al., 2016; Taburet et al., 2019). An optimized reference field (mean profiles of SSH) is used to compute SLA for missions with a repetitive orbit. The gridded SLA data are provided daily on a 1/4° grid.

The main differences between the two CMEMS products are: the number of satellites used, the implementation of the new GDR-E orbit standard (for missions: Jason-1, Jason-2, Cryosat-2, AltiKa, Jason-3 et Sentinel-2A), the improvement of the geophysical corrections (especially the *ocean_tide* correction) and the interpolation technique (especially in the coastal zones) in DT2018 compared to DT2014. This previous version uses the GDR-D orbit, which is less accurate than the GDR-E orbit, and does not include Sentinel-3A data (Taburet et al., 2019). The DT2018 errors at meso-scales are reduced by nearly 3 to 4% for regional products (up to 10% in coastal areas) compared to the DT2014. For the detailed descriptions of these two products, the reader is referred to the CMEMS web site, as well as to Pujol et al. (2016) and Taburet et al. (2019).

2.2 Realistic numerical model data

The numerical model used for our study is the oceanic component of the Nucleus for European Modeling of the Ocean program (NEMO3.6 STABLE, rev8019, see Madec, 2016). It solves the three dimensional primitive equations discretized on a C-grid with fixed vertical levels and a nesting capacity allowed by the AGRIF package (Adaptive Grid Refinement In Fortran; see Debreu and Blayo, 2002).

Sea level data from two NEMO configurations of the Tropical Atlantic Ocean have been used: *(1)* NEMO.1/4, available on 1/4° grids throughout the ETAO region and called the

parent grid (a very similar configuration is described in Hernandez et al., 2017), and *(2)* NEMO.1/12, with a fine resolution of 1/12° available in the tropical Atlantic ocean over a smaller domain (31°S–16°N; 25°W–African coasts), called the child grid. At each time step, the parent grid provides boundary conditions for the child grid and variables from the child grid are updated to the parent grid (see details in Jouanno et al. 2008). The coarse grid NEMO.1/4 is forced at its lateral open boundaries with daily outputs from the global GLORYS2V4 reanalysis from MERCATOR-OCEAN (https://www.mercator-ocean.fr/). The open boundary conditions radiate perturbations out of the domain and relax the model variables to 1 day averages of the global experiment. The tidal forcing is not taken into account. Atmospheric fluxes of momentum, heat, and freshwater are provided by bulk formulae (Large and Yeager, 2009): the model is forced with DRAKKAR Forcing Sets product (DFS5.2; Dussin et al., 2016) which is based on ERA-interim reanalysis and consists of 3-hour fields of wind speed, atmospheric temperature and humidity, and daily fields of long wave and short wave radiations and precipitation. The monthly climatological runoffof Dai and Trenberth (2002) is prescribed near the river mouths as a surface fresh-water flux with increased vertical mixing in the upper 10 m. The simulations are initialized with temperature and salinity from GLORYS2V4 on the 1st of January 1993 and performed over the period 1993 – 2015 with daily outputs.

2.3 Tide gauge data

The TG data come from the version 4.2 of the University of Hawaii Sea level Center database (UHSLC; https://uhslc.soest.hawaii.edu/). We used the hourly data, using a more rigorous data quality control and dedicated to research (Caldwell et al., 2015), which are available for 14 stations along the coast of the ETAO area (see the list in Table.1 and in Fig.1 showing the position of TGs along the West African coast). We have applied the *ocean_tide* and *DAC* corrections using a spectral analysis method from the *detidor function* and MOG2D-G/T-UGOm, respectively. The TGs present a lot of missing data over the altimetry period (1993 – present), before 2008 and especially before 2000 (see Table.1. Half of the TGs in the region are available only after 2000). Given the missing data on the time series of the 14 TGs before 2008, we decided to limit our study to the period January 2008 – December 2014, (corresponding also to the Jason 1 and 2 altimeter period), where TGs have the least amount of missing data. In addition, the data of recent altimeter missions (e.g. Jason-2) presents fewer errors (e.g: orbital error or instrumental errors) than their predecessors (e.g. Topex/Poseidon) (Watson et al., 2015; Dieng et al., 2017; Ablain et al., 2017).

3. Validation of altimetry and NEMO model data along the western African coast using the TG

3.1 Calculation of the sea level anomaly: SLA

The mean dynamic topographic (MDT) of Fig.1 was obtained by removing the geoid from the X-TRACK mean sea surface height (MSSH) calculated over the period 2008-2014. It shows strong sea-level rise in the equatorial band, more marked between 0 and 7°N, in connection with the Northern branch of the South Equatorial Current (Schott et al., 2004) and offshore below 20°S, influenced by the Southern branch of the South Equatorial Current (Schott et al., 2004). In the present paper, the main goal is to study the variability of the SLA using different data sets after the validation of these data over the same time period 2008-2014. The different datasets provide mean sea level fields based on different reference ellipsoid, geoid or local reference over land. *[1]* X-TRACK provides SLA time series between February 1993 and September 2016 and a MSSH calculated between cycles 17 and 868 (i.e., over the period February 1993 - April 2016). We reconstructed the SSH signal over this period by summing the MSSH and the SLA, the latter being calculated with respect to the Topex/Poseidon reference ellipsoid. *[2]* CMEMS provides a Dynamic Topographic (*DT)* which corresponds to the sea level relative to the geoid (GOCE geoid model; Mulet et al., 2013; Rio et al., 2014). *[3]* The NEMO model, like the CMEMS product, provides the DT with respect to a geoid. However, they do not use the same geoid data, the NEMO assuming a spherical earth (i.e., the geopotential surfaces are assumed to be spheres so that gravity is parallel to the earth's radius). Due to incomplete knowledge of the geoid at small-scale, the choice of the latter may lead to differences in regional and local DT (Dibarboure et al., 2011). *[4]* The TG observations track changes in sea level with a reference over land.

To overcome the different choices for sea level reference, we decided to consider *SLA* for the four datasets, obtained by removing the time average of *SSH*-or-*DT*, called *MSSH*-or-*MDT*, calculated over the period 2008 – 2014:

$$SLA = SSH - MSSH = DT - MDT \qquad (4)$$

where *DT* is the difference between the *SSH* and the *geoid*.

Similar methods for the SLA estimation have already been used in previous studies (e.g., Fenoglio-Marc et al., 2015; Jebri et al., 2016; Gómez-Enri et al., 2016, 2018 and 2019; Birol

et al., 2017; Salazar-Ceciliano et al., 2018; Taburet et al., 2019). Some are studies also compare the different products of DT by applying an additional offset to each sea level time series, chosen so that the average value is zero for the strating year (e.g., Risien and Strub, 2016; Idris et al., 2017). This allows to estimate sea level rise with respect to the reference year (in our case, the reference year would be 2008).

3.2 Comparison between the SLA products along the African coasts

In this section we compare X-TRACK, CMEMS/DT2014 and NEMO.1/4 SLA to TG using several standard statistical criteria or metrics such as correlation, standard deviation and RMS. We used the Taylor diagrams (Taylor, 2001) to represent these metrics on the same diagram. Taylor diagrams (Taylor, 2001) are designed to graphically indicate the degree of correspondence between different data sets, one taken as a reference (here the TG). It allows to represent three statistics (correlation, standard deviation and RMS error) on a single graph (see Fig.2 caption for detailed description). For better comparisons, we applied temporal and spatial optimal interpolation on grided data (CMEMS/DT2014 and NEMO.1/4) to match the position and time of X-TRACK measurements. A temporal interpolation is also applied to TG data to match the X-TRACK measurement dates. The three sub-regions are considered separately.

Fig.2a, Fig.2b and Fig.2c show the comparisons between the SLAs of X-TRACK, CMEMS/DT2014 and NEMO.1/4 model and the SLAs of the TGs (taken as references) from Dakar (Senegal region), Pointe Noire (Gulf of Guinea region) and Walvis Bay (Benguela region), respectively. We consider the track that passes closest to the TG and data are taken from the coast to 300 km offshore. For TGs located on islands (this is the case of the TGs of Palmeira and Sao Tome) we consider the altimetry data closest to the TG whereas for continental TGs we consider the altimetry data closest to the coast even if the altimetry track do not necessarily pass over the TG. Table 2 summarizes the results for all TGs. When comparing altimetry products and in-situ data, the products are considered to agree with the TGs when the correlation > 0.6, normalized standard deviation between 0.7 and 1.3 and normalized RMS < 0.8 (Ablain et al., 2016; Birol et al., 2017). For example, for the case of Dakar (see Fig.2a) these criteria correspond to a standard deviation of 6 cm and 8.5 cm for X-TRACK and TG, respectively and an RMS of the difference between X-TRACK and TG between 4 and 6 cm.

We note a good agreement of altimetry products and NEMO.1/4 model with TGs near the coast in the Senegal and Gulf of Guinea regions with correlations above 0.7 and normalized

RMS mainly lower than 0.8. Some of the areas are at the limit of our criteria (correlations slightly higher than 0.6 and normalized RMS slightly lower than 0.8), but this is most probably due to higher distances that separate the TGs to the nearest altimeter tracks. This is the case for example of Palmeira (see Table 2) where this distance can go up to more than 100 km (see the track and TG locations in Fig.1).

For the Benguela region (see Fig.2c and Table 2 in green color), there is a poor agreement between the altimetry products, the NEMO.1/4 model and the TGs. Indeed, correlations are well below 0.5 and normalized RMS are higher than 0.8. The further we go pole-ward, the more the agreement between the products and TGs decreases. Comparison of products with Granger Bay and Simon's Town TGs shows very weak agreements with correlations <0.3 or negative beyond a few tens of km. This result is not improved when the SLAs of X-Track, CMEMS/DT2014 and NEMO.1/4 model are compared to each other. This disagreement could be related to the combined effects of the position of the TGs (located in semi-closed bays), the altimeter geophysical corrections (e.g. *ocean_tide* and *DAC*) or the low spatial resolution of the NEMO.1/4 model.

Over the ETAO region, for the normalized standard deviation, we observe a better result for the X-TRACK data near the coast, as compared to CMEMS/DT2014 and NEMO.1/4, especially in the first 75 km (except for the first point along the track, less than 7 km away, due to the disturbance of the radar echoes of the satellite by land). However this is not the case for correlation and normalized RMS, because X-TRACK product is not filtered spatially along-track.

4. Spatial patterns of regional SLA correlation and RMS between different products and TGs

In this section, we will limit our analysis to one TG per region, selected for their quality with fewer missing data: Dakar’s TG for the Senegal area, Pointe Noire’s TG for the Gulf of Guinea and Walvis Bay for the Benguela area.

Fig.3 shows the correlation and the RMS of the difference between the SLA of X-TRACK and selected TGs, calculated over the 2008 – 2014 period. For both correlation and RMS, spatial patterns are different between the 3 study areas, denoting different dynamical behavior of each area. However, areas with strong correlations present also a low RMS. In the Gulf of Guinea, we observe a spatial coherence of X-TRACK SLA compared to TG over large distances, with correlations > 0.7 and RMS < 6 cm up to distances greater than 1000 km. This

can be related to rapidly propagating physical processes, such as equatorial Kelvin wave propagating eastward along the equator. For the Senegal region, the high correlations have very limited spatial patterns (< 300 km to the coast) compared to those of the Gulf of Guinea. In contrast, the correlation is low between the SLA of X-TRACK and Walvis Bay TG in the Benguela region (Fig.3). Interestingly, the best agreement is for track number 122, located along the coast but not the closest to the TG, with correlations reaching 0.45 to 0.55 over long distance northward of the TG (> 500 km from TG). We can deduce that this TG, located in a semi-closed bay (open to the north), only captures the part of the oceanic dynamics which is propagating southward, such as coastal trapped Kelvin waves, and that influences the coastal bay through its northern oceanic entrance.

To better observe and explain spatial patterns of correlation and RMS with the TGs in the three studied regions, we also considered the two other SLA data products from CMEMS/DT2014 and NEMO.1/4 non-interpolated on X-TRACK tracks. Figures 4a and 4b give the maps of correlation and RMS between the CMEMS/DT2014 and TG and between NEMO.1/4 and TG, respectively. These figures (Fig.3, Fig.4a and Fig.4b) show that the signal picked up by the Pointe Noire TG is mainly equatorial and homogeneous over very long distances (> 1000 km) and this signal is also observed in the altimeter products and the NEMO.1/4 simulation. On the other hand, the SLA signals captured by the Dakar and Walvis Bay TG are mainly coastal processes (over a width of less than 400 km from the coasts), such as coastal upwelling systems. We also note that the correlation along the coast is better between X-TRACK and Walvis Bay TG (for the track number 122, see Fig.3) compared to CMEMS/DT2014 (Fig.4a) and NEMO.1/4 (Fig.4b), however the agreement between all the products remains weak in the Benguela region. To take into account the possible lag in time associated with the distant locations of the TGs and the altimetric data, we also applied a 10-to-30 days lag-correlation between the SLA data from altimetry products (X-TRACK and CMEMS/DT2014) and NEMO model and the TG. This did not improve the agreement between altimetric products and TGs in the Benguela (the correlation remains below 0.6) or the Senegal and Gulf of Guinea regions (for which the agreements were already good). Time lag-correlation analysis were also performed to determine the direction of propagation of the physical signals around the TGs in the three studied regions. In the Senegal region, the SLA signal captured by the Dakar TG (which is mainly seasonal, see section 6) originates from North of the TG position and moves along the coast equator-ward, from 25°N to 6°N via Dakar within a coastal band of about 200 km to 300 km width, then moves westwards at

about 6°N. The NEMO.1/4 model and CMEMS/DT2014 product show that the signal correlated with the Dakar TG comes from the open ocean between 20°N and 25°N before moving along the coast equator-ward, which is not visible with X-TRACK. The ocean circulation that we describe with the altimetry and the NEMO model along the Senegalese coastlines between 20°N and 10°N is in agreement with the article by Nyoye et al. (2017) on the circulation of the Canary Current System based on a modeling approach. We observed that the signal picked up by the Pointe Noire TG (which is mainly seasonal and interannual, see section 6) comes from the equator and spreads eastward over a very large distance (> 1000 km) over a short time (< 20 days), then a part of the signal moves along the coast southward and can go up to 15°S. However, the altimeter shows that part of the signal goes also northward along the coast before encountering the Guinea Current near the coasts of Ghana. This northward signal is less marked with the NEMO model. This signal is very coherent with equatorial Kelvin waves propagating eastward toward African coasts and then transformed into coastal trapped waves propagating southward and northward (e.g. Cipollini et al., 1998; Bachèlery et al., 2015, Illig et al., 2018). Near Walvis Bay, the three products show that the correlated SLA signal captured by the TG is mostly coastal and propagates from the equator southward at least up to 30°S, the limit of our region.

Our results on the direction of propagation of SLA signals in the Gulf of Guinea and Benguela regions agree with the study of Bachèlery et al. (2016). They demonstrated using an oceanic model that, along the south-west coast of Africa (0° – 30°S), the dominant variability is associated with coastal trapped waves and is mainly controlled by the equatorial remote forcing (equatorial Kelvin waves) up to 15°S – 20°S at intra-seasonal time scale and up to 30°S at inter-annual time scales.

5. Impact of high resolution of NEMO model and CMEMS new version

In this section, we evaluate the performance of a 1/12 degree NEMO model (NEMO.1/12) and improved altimetry geophysical corrections for the latest version of CMEMS altimeter multi-mission product (CMEMS/DT2018, see section 2 for details). Table 3 compares the statistical analysis of the previous products (CMEMS/DT2014 and NEMO.1/4) and the new products (CMEMS/DT2018 and NEMO.1/12, indicated in red in table 3) with the TGs of Dakar, Pointe Noire and Walvis Bay. The given statistics were calculated by taking the average of the correlations and RMS over a distance of 100 km of the coast around the TGs.

Thanks to a better representation of coastal processes achieved with improved corrections and higher resolutions, we observe better correlations and lower RMS between the new products and TGs, throughout the ETAO region. However, these improvements are not of the same order of magnitude in our three study zones. In the Gulf of Guinea, NEMO.1/12 model and CMEMS/DT2018 allow for a slight improvement in the agreement with the TG as compared to NEMO.1/4 and CMEMS/DT2014, with an increase in correlation of 4% and a decrease in RMS of 5% near the coast. In the Senegal region, we note, with NEMO.1/12 (available below 16.75°N) and CMEMS/DT2018, a correlation increase of 4% and 6% and an RMS decrease of 18% and 20% near the coast, respectively. For the Benguela region, we observed on average over the whole area a correlation increase of 15% and 5% with NEMO.1/12 and CMEMS/DT2018, respectively. In terms of RMS the average improvement is of 8% with NEMO.1/12 and very low with CMEMS/DT2018 (less than 2%).
In summary, a higher spatial resolution and improved geophysical altimetry corrections near the coast improve the inter-comparison between the different products and TG in the ETAO region.

6. Spatio-temporal variability of SLA

In this section, the goal is to determine and understand the dominant spatio-temporal variability of the SLA in the ETAO region. As in the previous sections, we will limit our analysis to the three sub-regions (Senegal, gulf of Guinea, Benguela) and using TGs from Dakar, Pointe Noire and Walvis Bay.

Fig.5a, Fig.5b and Fig.5c show the Hovmüller diagrams (distance to the coast / time) of X-Track SLA tracks (track number 174, 185 and 235, respectively; see their positions on Fig.1) closest to the three TGs above, over 2008 – 2014 and for the first 500 km. These figures exhibit a clear seasonal signal for the 3 tracks, even if it is more marked for track 174 near Dakar (Fig.5a) with an annual variability visible from 500 km offshore up to the coast. In addition to the annual signal, track 185 near Pointe Noire (Fig.5b) shows semi-annual signals within the first 400 km from the coast and high frequencies (short periods) between 400 and 500 km from the coast. The track number 235 around Walvis Bay (Fig.5c) exhibits a lot of high frequencies mainly within the first 300 km from the coast.

To refine our analysis, we considered SLA time series at a point near the coast (about 15 km from the coast, where the series has the least possible missing data) for X-TRACK and NEMO.1/12 and CMEMS/DT2018. Both gridded products are interpolated on X-TRACK

tracks 174, 185 and 235. These time series as well as those of the 3 TGs are shown in Fig.6, which confirms the agreement between the different products near Dakar (with positive SLA between August and November and negative towards February) and Pointe Noire (with positive SLA between October and November then between February and March and negative towards June-July), but also their low correlation near Walvis Bay. We made a spectral analysis of these time series using FFT (Fast Fourier Transform) in order to observe the dominant signals for periods less than 2 years. This is illustrated in Fig.7 and the values of the maximum amplitudes and associated periods are listed in Table 4. We observe near Dakar that the signal is mainly annual for all 4 products (with amplitudes of about 8 to 9 cm which constitutes nearly half of the signal), even if there is a lower semi-annual and 122 days signal. Near Pointe Noire coast, the signal is annual and semi-annual for the 4 products, although the NEMO.1/12 model has a semi-annual signal higher than the annual one. We also observe a significant part of inter-annual variability and a signal at 120 days around Pointe Noire notably with altimetry and TG. In the case of Walvis Bay, unlike other regions, with the exception of the dominant annual signal, we note several strong high frequency signals near the coast with periods less than 100 days. These high frequency signals are more marked with X-TRACK and the NEMO.1/12 model.

To evaluate the spatial structure of the amplitude and time periods of the main variability modes over the whole ETAO region, we calculated the FFT of SLA time series from X-TRACK, CMEMS/DT2018 and NEMO.1/12 (with NEMO.1/4 above 16°N) at each point of the satellite tracks available in the ETAO region. Fig.8a, Fig.8b and Fig.8c respectively give the 1st, the 2nd and the 3rd dominant signal (in terms of amplitude) and their associated periods. We also added the FFT calculated from the SLA time series of the Dakar, Pointe Noire and Walvis Bay TGs. This confirms that SLA variations are primarily annual and semi-annual in the region, even if we observe a low interannual variability at the equator and high frequencies south of 10°S. The annual signal constitutes nearly half of the total signal variability near Dakar, against about 25% near Pointe Noire and less than 10% near Walvis Bay. We also note a good agreement between the 2 altimetry products (X-TRACK and CMEMS/DT2018) for amplitudes and periods of the dominant signals in the region. Fig.8a shows that the annual SLA signal is dominant throughout the region except in the northern Gulf of Guinea where the semi-annual cycle dominates (although it is only slightly higher than the annual cycle). Unlike altimetry data, the NEMO.1/12 model has a much wider semi-annual spatial pattern in the Gulf of Guinea and up to 10°S near the coast. In addition, the

NEMO.1/12 model also has smaller amplitudes. Altimetry and the NEMO.1/12 model also show interannual variability (400 to 650 days) on the equatorial band, although the amplitude is small with the NEMO.1/12 model (Fig.8c). Moreover this interannual variability is visible with NEMO only on a small part of the equatorial band contrary to the altimetry. This signal could be related to equatorial Kelvin waves that propagate eastward along the equator, as shown in several publications (e.g. Cipollini et al., 1998; Bachèlery et al., 2015; Illig et al., 2018).

7. Discussion

7.1 Validation of SLA products near the ETAO coasts

Compared to previous studies in the ETAO region, the originality of our work is the large number of TGs used.For instance, Verstraete and Park (1995) focus on a small area and use a single TG to validate the altimetry data near the Sao Tomé island. Our results offer a more synoptic view of the dynamics in the ETAO region. However, there are large areas along the ETAO coast not covered by the TG network (no TG between Dakar and Takoradi and between Pointe Noire and Walvis Bay, distant of more than 1500 km). In the Senegal region, our study is the first to compare and validate different SLA products including altimetry data near the coast. Studies on the sea level trend have been conducted in this region (e.g., Thoreux et al., 2018; Le Cozannet et al., 2015) but due to the limited number of TG available along the ETAO coast, more studies validate altimetry using video camera data installed near coastal cities in the region (e.g., Angnuureng et al., 2018; Abessolo-Ondoa et al., 2019). However, their time series remain short and present significant missing data due to maintenance problems of these facilities in these countries (Abessolo-Ondoa et al., 2016).

Another original contribution of our study is the combination of three complementary data types, namely the satellite (including X-TRACK dedicated to coastal oceanography and providing valid SLA measurements within the first 6 km from the coast), model data and in situ measurements (TG).

In this study, we show a very good agreement between altimetry, NEMO model and TG in the Senegal and Gulf of Guinea regions in terms of SLA variability. This is not the case in the Benguela region and is probably explained by the positions of TG located in semi-enclosed bays, which do not capture very well the physical signal coming from the ocean, but also by

the altimeter geophysical corrections (eg tide, DAC and/or SSB) and the too low spatial resolution of the gridded data (CMEMS and NEMO) to represent the variability in this region, dominated by high frequency small scale processes. We also show that high spatial resolution and improved altimeter geophysical corrections near the coast can significantly reduce data errors (about 10% for each) near the coast. For example, the X-TRACK algorithm dedicated to coastal application (measurements every 6 km and based on specific editing) improves the SLA data near the coast, especially over the first 50 km, and significantly reduces the standard deviation from the TG. This is consistent with Taburet et al. (2019) who showed that improved mesoscale geophysical corrections in altimetry products can reduce sea level measurement errors by up to 4% for regional products and up to 10% in coastal areas. However, efforts need to be strengthened in this direction (higher spatial resolution and improved geophysical altimetry corrections near the coast) for the Benguela region, where the agreement between different products remains weak compared to the other ETAO regions.

In the Gulf of Guinea region, oour results confirm Verstraete and Park (1995) who compared the Topex/Poseidon altimetry data with the Sao Tome TG data, between October 1992 and December 1993. Their time period was however shorter and the Topex/Poseidon altimetry data presents great uncertainties (orbit calculation and the Topex-A altimeter drift over 1993–1998) compared to the Jason-1/2/3 data (Watson et al., 2015; Dieng et al., 2017; Ablain et al., 2017). The latter estimated the impact of Topex-A altimetry drift on the measurement of global sea level trend, but also noted the improvements in terms of geophysical and instrumental corrections made to Jason altimeters since 2000s compared to Topex/Poseidon. An important scientific question remains concerning the impact of the Topex-A drift on the regional and local sea level, especially along the ETAO coasts.

In the Benguela region, Rubio et al. (2009) found an agreement between altimetry and the Regional Ocean Model System (ROMS) in terms of DT (sum of MDT and SLA) between the Luderitz and Cape Town positions. In our study , we show this is not the case for SLA. This can be explained by the high value of the MDT in this region with amplitude up to more than 0.5 m (as shown in Fig.1) in connection with the Benguela current and the South Equatorial Current (Schott et al., 2004). The SLA has smaller amplitudes (less than 0.2 m) in this region (see Fig.5c) and is associated to intermittent mesoscale structures in the Benguela upwelling system as well as with the Agulhas anticyclonic eddies (e.g. Rubio et al., 2009; Pegliasco et al., 2015; Aguedjou et al., 2019). The impact of the geoid error at mesoscale on the DT along the ETAO coasts also needs to be studied in order to be confident in the DT spatial variability.

7.2 Temporal variability of SLA

Another original contribution of our study is the comparison of the dominant frequencies of all products.

We showed that the annual and semi-annual signals dominate the ETAO region, even if we observe smaller amplitudes with NEMO compared to the altimetry data. This confirms earlier studies in this region (e.g., Verstraete and Park, 1995; Schouten et al., 2005; Rubio et al., 2009; Jouanno et al., 2011; Melet et al.216), which used altimetry or the oceanic models. In addition, we show that the semi-annual signal may be more important than the annual signal in the northern part of the Gulf of Guinea (the NEMO model identifying an even much larger zone). This could be related to modulation of winds and precipitations associated with the African monsoon, which has a high semi-annual variability with long spring rains (March-April-May) and short fall rains (October-November-December) (Bielli et al., 2009; Janicot et al., 2016). Altimetry products also show an important inter-annual signal in the equatorial band, with smaller amplitudes in the NEMO model. The origin of this difference between the altimetry and the NEMO model remains to be explained.

The recent study of Melet et al. (2016) off shore of Cotonou (northern part of the Gulf of Guinea) over the period 1993-2012, examines the relative contribution of the processes responsible for the coastal sea level variability (mainly the ocean tides, atmospheric pressure, wave and swell effects and mesoscale activity) with strong sub-seasonal to interannual variability. Our study allows to isolate the contribution of mesoscale processes, as we focus on SLA, corrected from ocean tide, DAC and SSB. These corrections have a strong impact near the coast for high frequency variability (daily to monthly period) and amplitudes of the order of one meter for ocean tide (Melet et al., 2016; Birol et al., 2017), which can mask the SLA signal (with amplitudes lower than 25 cm).

Our study thus highlights the different physical processes that can influence SLA near the coast. In the Gulf of Guinea, we have shown a spatial coherence between the SLA from altimetry and NEMO model over long distances of up to 1000 km from the coast, related to the propagation of Kelvin waves along the equator with interannual and seasonal variability (Bachèlery et al., 2016; Illig et al., 2018; Illig and Bachèlery, 2019). This is also consistent with the recent study of Woodworth et al. (2019) suggesting that coastal variability are not always as associated with short spatial scales but can result from signals generated 1000s km offshore and reaching the coast, then propagating along it. In contrast, coastal upwelling

signals (Senegal and Benguela) are mostly trapped along the coast with a width of less than a few 100s km. However, the identification and exact origin of these physical processes (mainly annual) remains to be identified.

8. Conclusion

The 7-year comparison of SLA data (2008-2014) from altimetry (X-TRACK and CMEMS/DT2018), the NEMO.1/12 model shows a good agreement with TGs near the coast of West Africa, in Senegal and Gulf of Guinea regions. This result indicates that sea-level time series from these products can be used to estimate mesoscale geostrophic currentsand study coastal dynamics in these two regions.

In contrast, despite new improvements in altimetry products or using a high resolution NEMO model (particularly in terms of geophysical corrections and spatial resolution), agreements between different SLA products are still poor in the Benguela region. This suggests that efforts need to be intensified in improving geophysical corrections and increasing temporal and spatial resolution near the coast, particularly in the Benguela region, to further improve SLA products. A first step can be to use the very high resolution T-UGOm model (for the tide and DAC corrections, with a spatial resolution of a few meters and an hourly temporal resolution) and X-TRACK-ALES 20 Hz SLA products, processed by the CTOH in the context of the bridging phase of the ESA's climate change initiative sea-level project, which combines the two altimeter processing methods (Editing and Retraking) and allows to go even closer to the coast, less than 1 km for the best case (Marti et al. 2019). We also emphasize the importance and the need to maintain and complete the in-situ observation network (e.g., TGs) along the West African coast, where there still exist spatial and temporal measurement gaps. These improvements will enable us to better observe and analyze the meso-scale activity near these coasts.

Acknowledgements

Habib Boubacar DIENG is supported by the Alti-ETAO project funded by the French National Center for Space Studies (CNES) through the Ocean Surface Topography Science Team (OSTST) and by the French National Institute of Sciences of the Universe (INSU/CNRS). We thank the CTOH for the X-TRACK data (http://ctoh.legos.obs-mip.fr/), Copernicus for their CMEMS data (http://marine.copernicus.eu/), University of Hawaii for the TG data (https://uhslc.soest.hawaii.edu/) and Jouanno et al. (2016) for their simulation of the NEMO model.

References

Abessolo-Ondoa G., Almar R., Castelle B., Testut L., Léger F., Sohou Z., Bonou F., Bergsma E.W. J., Meyssignac B. and Larson M. (2019), Sea Level at the Coast from Video-Sensed Waves: Comparison to Tidal Gauges and Satellite Altimetry. *American Meteorological Society* doi:10.1175/JTECH-D-18-0203.1

Abessolo Ondoa G, Almar R, Kestenare E, Bahini A, Houngue G-H, Jouanno J, Du Penhoat Y, Castelle B, Melet A, Meyssignac B, Anthony E, Laibi R, Alory G, Ranasinghe R (2016), Potential of video cameras in assessing event and seasonal coastline behaviour: a case study at Grand Popo, Benin (Gulf of Guinea). *J. Coast Res.*, 75:442–446, doi:10.2112/SI75-089.1

Ablain M., R. Jugier, L. Zawadki et al. (2017), The TOPEX-A Drift and Impacts on GMSL Time Series. AVISO Website, October 2017. https://meetings.aviso.altimetry.fr/fileadmin/user_upload/tx_ausyclsseminar/files/Poster_OSTST17 GMSL_Drift_TOPEX-A.pdf.

Ablain M., Legeais J. F., Prandi P., Marcos M., Fenoglio-Marc L., Dieng H. B., Benveniste J. and Cazenave A. (2016), Altimetry-based sea level at global and regional scales. *Surv. Geophys*. DOI 10.1007/s10712-016-9389-8.

Aguedjou H. M. A, Dadou I., Chaigneau A., Morel Y., Alory G., 2019, Eddies in the Tropical Atlantic Ocean and their seasonal variability, in revision for *Geophys. Res. Let.* Angnuureng D. B., Appeaning Addo K., Almar R. and Dieng H. B. (2018), Influence of sea level variability on a micro-tidal beach. *Nat. Hazards*, volume 68, doi.org/10.1007/s11069-018-3370-4

Bachèlery, M.-L., S. Illig, and I. Dadou (2016), Forcings of nutrient, oxygen, and primary production interannual variability in the southeast Atlantic Ocean, *Geophys. Res. Lett.*, 43, 8617–8625, doi:10.1002/2016GL070288.

Baquet E., (2018). Ondes internes solitaires dans le Golfe de Guinée : Cartographie et modélisation. *Université de Bretagne Occidentale.*

Bielli S., H. Douville and B. Pohl (2009), Understanding the West African monsoon variability and its remote effects: an illustration of the grid point nudging methodology. *Clim. Dyn.* DOI 10.1007/s00382-009-0667-8

Birol, F., Fuller, N., Lyard, F., Cancet, M., Niño, F., Delebecque, C., Fleury, S., Toublanc, F., Melet, A., Saraceno, M., Léger, F. (2017), Coastal applications from nadir altimetry: Example of the X-TRACK regional products. Advances in Space Research 59, 936–953. https://doi.org/10.1016/j.asr.2016.11.005

Bonnefond P., Exertier P., Laurain O., Guillot A., Picot N., Cancet M. & Lyard F. (2015) SARAL/AltiKa Absolute Calibration from the Multi-Mission Corsica Facilities, *Marine Geodesy*, 38:sup1, 171-192, DOI: 10.1080/01490419.2015.1029656

Brandt, P., G. Caniaux, B. Bourlès, A. Lazar, M. Dengler, A. Funk, V. Hormann, H. Giordani and F. Marin. (2010), Equatorial upper-ocean dynamics and their interaction with the West African monsoon. *Atmospheric Science Letters*, 12 (1), p. 24-30. ISSN 1530-261X.

Caldwell, P. C., M. A. Merrifield, P. R. Thompson (2015), Sea level measured by tide gauges from global oceans — the Joint Archive for Sea Level holdings (NCEI Accession 0019568), Version 5.5, *NOAA National Centers for Environmental Information*, Dataset, doi:10.7289/V5V40S7W.

Carrère, L. and Lyard F., (2003), Modelling the barotropic response of the global ocean to atmospheric wind and pressure forcing – comparisons with observations, *Geophys. Res. Let.*, 30(6), pp 1275.

Carrère L., F. Lyard, M. Cancet, A. Guillot, L. Roblou (2012), FES2012: A new global tidal model taking taking advantage of nearly 20 years of altimetry, *Proceedings of meeting "20 Years of Altimetry"*, Venice 2012.

Cipollini P., D. Cromwell and G. D. Quartly (1998) Observations of Rossby wave propagation in the Northeast Atlantic with TOPEX/POSEIDON altimetry; *Advances in Space Research*, 22(11): 1553-1556 https://doi.org/10.1016/S0273-1177(99)00069-1

Cipollini P., Calafat F.M., Jevrejeva S., Melet A. and Prandi P., (2017). Monitoring Sea Level in the Coastal Zone with Satellite Altimetry and Tide Gauges. *Surv. Geophys.*, 38: 33. https://doi.org/10.1007/s10712-016-9392-0

Dai A. and Trenberth K. (2002) Estimates of freshwater discharge from continents: latitudinal and seasonal variations. *Journal of Hydrometeorology*, 3: 660-687.

Djakouré, S., P. Penven, B. Bourlès, J. Veitch, and V. Koné, (2014). Coastally trapped eddies in the north of the Gulf of Guinea. *J. Geophys. Res. Oceans*, 119, 6805–6819, doi:https://doi.org/10.1002/2014JC01

Djakouré, S., P. Penven, B. Bourlès, V. Koné and J. Veitch (2017). Respective Roles of the Guinea Current and Local Winds on the Coastal Upwelling in the Northern Gulf of Guinea. *Journal of Physical Oceanography*, 47, 1367–1387, DOI: 10.1175/JPO-D-16-0126.1

Dieng, H.B, A. Cazenave, B. Meyssignac et al. (2017). New estimate of the current rate of sea level rise from a sea level budget approach, *Geophysical Research Letters*, 44, doi:10.1002/
730 2017GL073308.

Debreu L. and Blayo, E. (2002). AGRIF: Adaptive Grid Refinement In Fortran. [Research Report] RT-0262, *INRIA*., pp.16, inria-00069912.

Dibarboure, G., Pujol, M.-I., Briol, F., Le Traon, P.-Y., Larnicol, G., Picot, N., Mertz, F., Escudier, P., Ablain, M., and Dufau, C. (2011), Jason-2 in DUACS: first tandem results and impact on processing and products, Mar. Geod., OSTM Jason-2 Calibration/Validation Special Edition – Part 2, 34, 214–241, doi:10.1080/01490419.2011.584826, 2011.

Doi, T., Tozuka, T., & Yamagata, T. (2009). Interannual variability of the Guinea Dome and its possible link with the Atlantic meridional mode. *Climate Dynamics*, 33(7-8), 985-998. doi: 10.1007/s00382-009-0574-z

Doi, T., Tozuka, T., & Yamagata, T. (2010). The Atlantic meridional mode and its coupled variability with the Guinea Dome. Journal of Climate, 23(2), 455-475. doi: 10.1175/2009JCLI3198.1

Dussin, R., Barnier, B., and Brodeau, L. (2016), Up-dated description of the DFS5 forcing data set: The making of Drakkar forcing set DFS5, DRAKKAR/MyOcean Rep. 01-04-16, *Lab. of Glaciol. and Environ. Geophys.*, Grenoble, France.

Fenoglio-Marc L., Dinardo S., Scharroo R., Roland A., Dutour Sikiric M., Lucas B., Becker M., Benveniste J. and Weiss R. (2015), The German Bight: A validation of CryoSat-2 altimeter data in SAR mode. *Advances in Space Research*, 55 (2015) 2641–2656 doi:10.1016/j.asr.2015.02.014

Gonzalez, C. J.; Passaro, M.; Vignudelli, S.; Alvarez, O. (2019). Wind-induced cross-strait sea level variability in the Strait of Gibraltar from coastal altimetry and in-situ measurements ; *Remote sensing of environment*, Vol.221, p.596-608, DOI**:**10.1016/j.rse.2018.11.042

Gómez-Enri, J., Cipollini, P., Passaro, M., Vignudelli, S., Tejedor, B., Coca, J., (2016). Coastal altimetry products in the Strait of Gibraltar. IEEE T. *Geosci. Remote* 54 (9), 5455–5466. doi:10.1109/TGRS.2016.2565472.

Gómez-Enri, J., Vignudelli, S., Cipollini, P., Coca, J. & Gonzalez, C. J. (2018). Validation of CryoSat-2 SIRAL sea level data in the Eastern continental shelf of the Gulf of Cadiz. *Advances in Space Research*, 62 (2018) 1405–1420, doi:10.1016/j.asr.2017.10.042

Herbert, G., B. Bourle`s, P. Penven, and J. Grelet (2016), New insights on the upper layer circulation north of the Gulf of Guinea. *J. Geophys. Res. Oceans*, 121, 6793–6815, doi:10.1002/2016JC011959.

Hernandez O., J. Jouanno, V. Echevin, and O. Aumont (2017). Impacts of chlorophyll concentrations on the Tropical Atlantic Ocean. *J. Geophys. Res. Oceans*, doi:10.1002/2016JC012330

Idris N.H., Deng X., Din A.H.Md. and Idris N.H. (2017). CAWRES: A Waveform Retracking Fuzzy Expert System for Optimizing Coastal Sea Levels from Jason-1 and Jason-2 Satellite Altimetry Data. *Remote Sens.* 2017, 9, 603; doi:10.3390/rs9060603

Illig S., Bachelery M-L. and Cadier E. (2018), Subseasonal coastal-trapped wave propagations in the Southeastern Pacific and Atlantic Oceans : 2. Wave characteristics and connection with the equatorial variability. *J. Geophys. Res.*, 123, 3942–3961. https://doi.org/10.1029/2017JC013540

Illig, S. & M.L. Bachèlery, (2019): Propagation of Subseasonal Equatorially-Forced Coastal Trapped Waves down to the Benguela Upwelling System. *Nature - Sci Rep.*, 9, 5306. doi: 10.1038/s41598-019-41847-1

Janicot S., A. Giannini, F-M. Kamga et al., (2016) Report of the discussion group on the African monsoon: CLIVAR Panels. http://www.clivar.org/african-monsoon

Jebri, F., F. Birol, B. Zakardjian,J. Bouffard, and C. Sammari (2016),Exploiting coastal altimetry to improvethe surface circulation scheme overthe central Mediterranean Sea, *J.Geophys. Res. Oceans*,121, 4888–4909,doi:10.1002/2016JC011961.

Jouanno, J., J. Sheinbaum, B. Barnier, J.M. Molines, L. Debreu, et F. Lemarié, (2008). The mesoscale variability in the Caribbean Sea. Part I : simulations and characteristics with an embedded model. *Ocean Modelling*, 23, 82-101.

Jouanno, J., F. Marin, Y. du Penhoat, J. Sheinbaum, and J.- M. Molines (2011), Seasonal heat balance in the upper 100 m of the equatorial Atlantic Ocean. *J. Geophys. Res.*, 116, C09003, doi:10.1029/2010JC006912.

Jouanno, J., O. Hernandez, E. Sanchez-Gomez (2017), Equatorial Atlantic interannual variability and its relation to dynamic and thermodynamic processes, *In Earth System Dynamics*, Copernicus GmbH, volume 8.

Kumar, R., Sharma, R., Singh, R.P. et al., (2017) SARAL/AltiKa Mission: Applications Using Ka-band Altimetry. *Proc. Natl. Acad. Sci., India, Sect. A Phys. Sci.* 87: 581. https://doi.org/10.1007/s40010-017-0436-8

Large, W. G. and Yeager, S. (2009) The global climatology of an interannually varying air–sea flux data set. *Clim. Dynam.*, 33, 341–364, https://doi.org/10.1007/s00382-008-0441-3.

Le Cozannet, G. Raucoules, D. Wöppelmann, G.Garcin, M. Da Sylva, S.Meyssignac, B. Gravelle, M. Lavigne F. (2015). Vertical ground motion and historical sea-level records in Dakar (Senegal)**.** *Environ. Res. Lett.*, 10 (2015), Article 084016, 10.1088/1748-9326/10/8/084016

Lee, T., Lagerloef, G., Gierach, M. M., Kao, H. -Y., Yueh, S., and Dohan, K., (2012), Aquarius reveals salinity structure of tropical instability waves. *Geophys. Res. Lett.*, 39, L12610. http://dx.doi.org/10.1029/2012GL052232

Liu W-C. and Huang W-C. (2019). Influences of sea level rise on tides and storm surges around the Taiwan coast. *Continental Shelf Research* 173 (2019) 56–72, doi:10.1016/j.csr.2018.12.009

Marijan Grgić, Robert Steven Nerem & Tomislav Bašić (2017). Absolute Sea Level Surface Modeling for the Mediterranean from Satellite Altimeter and Tide Gauge Measurements, *Marine Geodesy*, 40:4, 239-258, DOI: 10.1080/01490419.2017.1342726

Marti, F., A., Cazenave, F., Birol, M., Passaro, F., Léger, F., Niño, R., Almar, J., Benveniste, J-F., Legeais (2019) Altimetry-based sea level trends along the coasts of Western Africa. *Advances in Space Research*, doi: https://doi.org/10.1016/j.asr.2019.05.033

Melet, A., Almar, R., & Meyssignac, B. (2016). What dominates sea level at the coast: a case study for the Gulf of Guinea. Ocean Dynamics, 66(5), 623-636.

Mulet, S., Rio, M. H., Greiner, E., Picot, N., and Pascual, A. (2013), New global Mean Dynamic Topography from a GOCE geoid model, altimeter measurements and oceanographic in-situ data, OSTST Boulder USA 2013, available at: http://www.aviso.altimetry.fr/fileadmin/documents/OSTST/2013/oral/mulet_MDT_CNES_CLS13.pdf

Ndoye, S., X. Capet, P. Estrade, B. Sow, E. Machu, T. Brochier, J. Döring, and P. Brehmer (2017), Dynamics of a "low-enrichment high-retention" upwelling center over the southern Senegal shelf, *Geophys. Res. Lett.*, 44, 5034–5043, doi:10.1002/2017GL072789.

Passaro, M., Cipollini, P., Vignudelli, S., Quartly, G. D., Snaith, H.M. (2014) ALES: a multi-mission adaptive subwaveform retracker for coastal and open ocean altimetry. *Remote Sens. Environ.*, 145, pp. 173-189, 10.1016/j.rse.2014.02.008

Peng F. and Deng X. (2018). Validation of Improved Significant Wave Heights from the Brown-Peaky (BP) Retracker along the East Coast of Australia. *Remote Sens.* 2018, 10, 1072; doi:10.3390/rs10071072

Pujol, M.-I., Faugère, Y., Taburet, G., Dupuy, S., Pelloquin, C., Ablain, M., and Picot, N. (2016). DUACS DT2014: the new multi-mission altimeter data set reprocessed over 20 years. *Ocean Sci.*, 12, 1067-1090, http://doi.org/10.5194/os-12-1067-2016, 2016.

Richter I, Xie SP, Behera SK, Doi T, Masumoto Y (2014) Equatorial Atlantic variability and its relation to mean state biases in CMIP5. *Clim. Dyn.*, 42:171–188, doi:10.1007/s00382-012-1624-5

Risien C.M. & Strub P.T (2016). Blended sea level anomaly fields with enhanced coastal coverage along the U.S. West Coast. *Scientific data*. Vol.3 DOI: 10.1038/sdata.2016.13

Rio, M.-H., S. Mulet, and N. Picot (2014), Beyond GOCE for the ocean circulation estimate: Synergetic use of altimetry, gravimetry, and in situ data provides new insight into geostrophic and Ekman currents, Geophys. Res. Lett., 41, doi:10.1002/2014GL061773.

Roblou, L., Lamouroux, J., Bouffard, J., Lyard, F., Le He´naff, M., Lombard, A., Marsalaix, P., De Mey, P., Birol, F., (2011), Postprocessing altimeter data toward coastal applications and integration into coastal models. In: Vignudelli, S., Kostianoy, A.G., Cipollini, P., Benveniste, J. (Eds.), Coastal Altimetry. *Springer, Berlin Heidelberg* (Chapter 9).

Ruiz Etcheverry L.A., Saraceno M., Piola A.R., Valladeau G. and Möller O.O. (2015). A comparison of the annual cycle of sea level in coastal areas from gridded satellite altimetry and tide gauges. *Continental Shelf Research* 92 (2015) 87–97, .doi:10.1016/j.csr.2014.10.006

Salazar-Ceciliano J., Trasviña-Castro A. and González-Rodríguez E. (2018). Coastal currents in the Eastern Gulf of Tehuantepec from coastal altimetry. *Advances in Space Research*, 62 (2018) 866–873 **DOI:** 10.1016/j.asr.2018.05.033

Schouten M.W., Matano R.P. and Strub T.P. (2005), A description of the seasonal cycle of the equatorial Atlantic from altimeter data. *Deep-Sea Research I* 52 (2005) 477–493, doi:10.1016/j.dsr.2004.10.007

Simon J. Holgate, Andrew Matthews, Philip L. Woodworth, Lesley J. Rickards, Mark E. Tamisiea, Elizabeth Bradshaw, Peter R. Foden, Kathleen M. Gordon, Svetlana Jevrejeva, and Jeff Pugh (2013) New Data Systems and Products at the Permanent Service for Mean Sea Level. Journal of Coastal Research: Volume 29, Issue 3: pp. 493 – 504. doi:10.2112/JCOASTRES-D-12-00175.1.

Taburet, G., Sanchez-Roman, A., Ballarotta, M., Pujol, M.-I., Legeais, J.-F., Fournier, F., Faugere, Y., and Dibarboure, G.: DUACS DT-2018: 25 years of reprocessed sea level altimeter products. *Ocean Sci. Discuss.*, https://doi.org/10.5194/os-2018-150, in review, 2019.

Thoreux, T.; Sakho, I.; Sall, M.; Testut, L., and Woppelmann, G. (2018). Trends in sea level around the Cap Vert peninsula, Senegal. In: Almar, R.; Almeida, L.P.; Trung Viet, N., and Sall, M. (eds.), Tropical Coastal and Estuarine Dynamics. *Journal of Coastal Research, Special* Issue No. 81, pp. 10–13. Coconut Creek (Florida), ISSN 0749-0208.

Schott, F. A., Zantopp, R., Stramma, L., Dengler, M., Fischer, J. and Wibauz, M. (2004) Circulation and deep-water export at the western exit of the subpolar North Atlantic. *J. Phys. Ocean.*, 34, pp. 817-843

Tseng K. H., Kuo-Hsin Tseng, C. K. Shum, Yuchan Yi, William J. Emery, Fellow, IEEE, Chung-Yen Kuo, Hyongki Lee, and Haihong Wang (2014). "The improved retrieval of coastal sea surface heights by retracking modified radar altimetry waveforms," IEEE Trans. *Geosci. Remote Sens.*, vol. 52, no. 2, pp. 991–1001, Feb. 2014.

Verron, J., Sengenes, P., Lambin, J., Noubel, J., Steunou, N., Guillot, A., Picot, N., Coutin-Faye, S., Sharma, R., Gairola, R. M., Raghava Murthy, D.V.A., Richman, J.G., Griffin, D., Pascual, A., Rémy, F., Murthy, D.R. (2015) The SARAL/AltiKa altimetry satellite mission. *Mar. Geodesy*, 38, pp. 2-21, 10.1080/01490419.2014.1000471

Verstraete, J. M., & Park, Y. H. (1995). Comparison of TOPEX/POSEIDON altimetry and in situ sea level data at Sao Tome Island, Gulf of Guinea. Journal of Geophysical Research: Oceans, 100(C12), 25129-25134.

Vignudelli, S., Kostianoy, A. G., Cipollini, P. Benveniste, J. (2011) Coastal Altimetry. *Springer* ISBN 978-3-642-12796-0.

Vu, P. L., Frappart, F., Darrozes, J., Marieu, V., Blarel, F., Ramillien, G., Bonnefond, P., Birol, F. (2018), Multi-Satellite Altimeter Validation along the French Atlantic Coast in the Southern Bay of Biscay from ERS-2 to SARAL. *REMOTE SENSING*, Vol.10(1) DOI: 10.3390/rs10010093

Watson, C. S., N. J. White, J. A. Church, M. A. King, R. J. Burgette, and B. Legresy (2015), Unabated global mean sea level over the satellite altimeter era. *Nat. Clim. Change*, doi:10.1038/NCLIMATE2635.

Woodworth P.L., Melet A., Marcos M., Ray R.D., Wöppelmann G., Sasaki Y.N., Cirano M., Hibbert A., Huthnance J.M., Monserrat S. and Merrifield M.A. (2019). Forcing Factors Affecting Sea Level Changes at the Coast. *Surveys in Geophysics*, doi:10.1007/s10712-019-09531-1

Wunsch and Stammer. (1997), Atmospheric loading and the oceanic "inverted barometer" effect. *Reviews of Geophysics*, 35 (1), pp. 79-107, https://doi.org/10.1029/96RG03037

Table.1: List of the 14 TGs available in the ETAO region, with their position and temporal coverage. Missing data for more than 3 consecutive months are considered as temporal gaps.

TG	Latitude (°)	Longitude (°)	Periods (month/year)
Nouakchott (Mauritania)	17.590	-16.020	01/2007 – 02/2008 ; 06/2008 – 02/2015
Palmeira (Cabo verde)	16.750	-22.983	02/2000 – 01/2001 ; 05/2001 – 02/2007 ; 10/2007 – 10/2016
Dakar (Senegal)	14.683	-17.416	01/1996 – 05/2003 ; 10/2007 – 10/2016
Takoradi (Ghana)	04.884	-01.745	01/2007 – 08/2007 ; 01/2008 – 04/2009 ; 01/2010 – 03/2010 ; 03/2011 – 08/2012
Lagos (Nigeria)	06.417	03.450	11/2008 – 04/2009
Port Sonara (Cameroon)	04.000	09.080	06/2008 – 06/2011
Sao Tome (Sao Tome)	00.201	06.434	08/2004 – 05/2007 ; 09/2007 – 08/2010
Pointe Noire (Congo)	-04.783	11.833	09/2008 – 06/2014
Walvis Bay (Namibia)	-22.930	14.500	01/1993 – 04/1993 ; 07/1994 – 12/1995 ; 01/1997 – 07/1997 ; 11/1997 – 11/1998 ; 05/2008 – 02/2011 ; 06/2011 – 02/2016
Luderitz (Namibia)	-26.6300	15.1500	01/1993 – 11/1993 ; 02/1996 – 09/1996 ; 01/1997 – 06/1997 ; 10/1997 – 12/1998 ; 05/2008 – 07/2012 ; 02/2013 – 10/2015
Port Nolloth (South Africa)	-29.257	16.868	01/2000 – 05/2000 ; 02/2001 – 08/2003 ; 08/2004 – 05/2006 ; 09/2006 – 05/2016
Saldanha Bay (South Africa)	-33.067	18.000	01/1993 – 12/1997 ; 05/2000 – 12/2001 ; 04/2002 – 08/2011 ; 02/2013 – 08/2016
Granger Bay (South Africa)	-33.9053	18.4400	01/1993 – 02/1994 ; 10/1994 – 12/1996 ; 07/1997 – 12/1997 ; 03/2001 – 12/2007 ; 04/2008 – 03/2010 ; 04/2013 – 10/2016
Simons Town (South Africa)	-34.1870	18.4400	01/1993 – 12/1995 ; 07/1997 – 12/1998 ; 02/2001 – 06/2002 ; 01/2003 – 06/2011 ; 02/2013 – 10/2016

Table.2: Comparison of the 3 products (X-TRACK, CMEMS/DT2014 and NEMO.1/4) with each TG in the 3 different zones of ETAO region. Statistics are calculated over the period 2008-2014. Agreement with the reference (TGs) is considered good when the correlation > 0.6, normalized standard deviation between 0.7 and 1.3 and normalized RMS < 0.8. The bold-red values indicate that these statistical criteria are not met.

Region	TG	Max correlation			Min normalized RMS (refereed in 0)			Min normalized standard deviation (refereed in 1)		
		X-TRACK	CMEMS	NEMO	X-TRACK	CMEMS	NEMO	X-TRACK	CMEMS	NEMO
Senegal	Nouakchott	0.73	0.75	0.70	0.71	0.66	0.73	0.95	0.92	0.70
	Palmeira	0.61	0.74	0.64	**0.92**	0.67	0.77	1.00	0.91	0.80
	Dakar	0.85	0.92	0.90	0.52	0.40	0.46	0.96	0.87	0.79
Gulf of Guinea	Takoradi	0.79	0.90	0.82	0.67	0.42	0.58	1.00	0.92	0.86
	Lagos	0.85	0.92	0.92	0.52	0.42	0.55	0.99	0.73	**0.62**
	Port Sonara	0.72	0.77	0.64	0.77	0.65	0.77	1.00	0.84	**0.69**
	Sao Tome	0.70	0.70	0.61	0.72	0.74	**0.81**	0.81	**0.57**	**0.47**
	Pointe Noire	0.86	0.90	0.82	0.57	0.43	0.58	1.00	0.88	0.79
Benguela	Walvis Bay	**0.51**	0.63	**0.51**	**0.98**	0.78	**0.87**	1.00	**0.46**	0.81
	Lüderitz	**0.50**	**0.52**	**0.41**	**1.00**	**0.85**	**0.94**	1.00	**0.68**	0.70
	Port Nolloth	**0.42**	**0.30**	**0.18**	**0.98**	**0.95**	**1.02**	0.81	**0.48**	**0.45**
	Saldanha Bay	**0.34**	**0.34**	**0.24**	**1.10**	**0.95**	**1.08**	1.00	1.00	1.05
	Granger Bay	**0.18**	**0.15**	**0.30**	**1.02**	**1.03**	**0.96**	0.98	**0.45**	1.12
	Simons Town	**0.30**	**0.28**	**0.30**	**0.91**	**0.93**	**0.88**	1.00	0.98	1.00

Table.3: Metrics of CMEMS/DT2018, CMEMS/DT2014, NEMO.1/4 and NEMO.1/12 with the TGs of Dakar, Pointe Noire and Walvis Bay, calculated over the period 2008-2014. Statistics are calculated taking the average of the correlations and RMS over a distance of 100 km off the coast around the TGs.

TG	Correlation				RMS (cm)			
	CMEMS/DT2014	CMEMS/DT2018	NEMO.1/4	NEMO.1/12	CMEMS/DT2014	CMEMS/DT2018	NEMO.1/4	NEMO.1/12
Dakar	0.83	0.88	0.84	0.87	**4.9**	4.1	4.5	3.8
Pointe Noire	0.85	0.88	0.81	0.84	4.4	4.2	4.9	4.6
Walvis Bay	0.41	0.43	0.41	0.47	5.3	5.2	5.3	4.9

Table.4: 1st, 2nd and 3rd maximums of SLA FFT amplitudes with the corresponding periods calculated over the period 2008-2014 with the different products (SLA points are located 15 km from the coast).

Data to 15 km from the coasts		Amplitude (cm)			Periods (days)		
		Dakar	Pointe Noire	Walvis Bay	Dakar	Pointe Noire	Walvis Bay
first maximum	TG	9.49	5.44	3.51	365	365	366
	X-TRACK	8.41	6.50	2.62	365	365	365
	CMEMS/DT2018	8.47	6.60	2.02	365	365	366
	NEMO.1/12	7,35	5.27	1.87	365	182.5	365
2 maximum	TG	2.71	3.43	1.92	182.5	182.5	641
	X-TRACK	2.36	4.92	1.67	182.5	182.5	69
	CMEMS/DT2018	2.50	4.96	1.00	182.5	182.5	641
	NEMO.1/12	2.95	4.45	1.27	182.5	365	95
3 maximum	TG	2.04	1.84	1.50	122	638.5	182.5
	X-TRACK	1.77	2.27	1.67	122	638.5	47
	CMEMS/DT2018	1.74	2.52	0.91	122	639	51
	NEMO.1/12	1.39	1.38	1.23	122	639	48

Figure Captions

Fig.1: Map of mean dynamic topography (MDT) (January 2008 – December 2014) calculated with XTRACK data. The white circles stand for the TG positions along the West Africa coasts between 35°S and 25°N. The satellite track numbers closest to the TG are indicated.

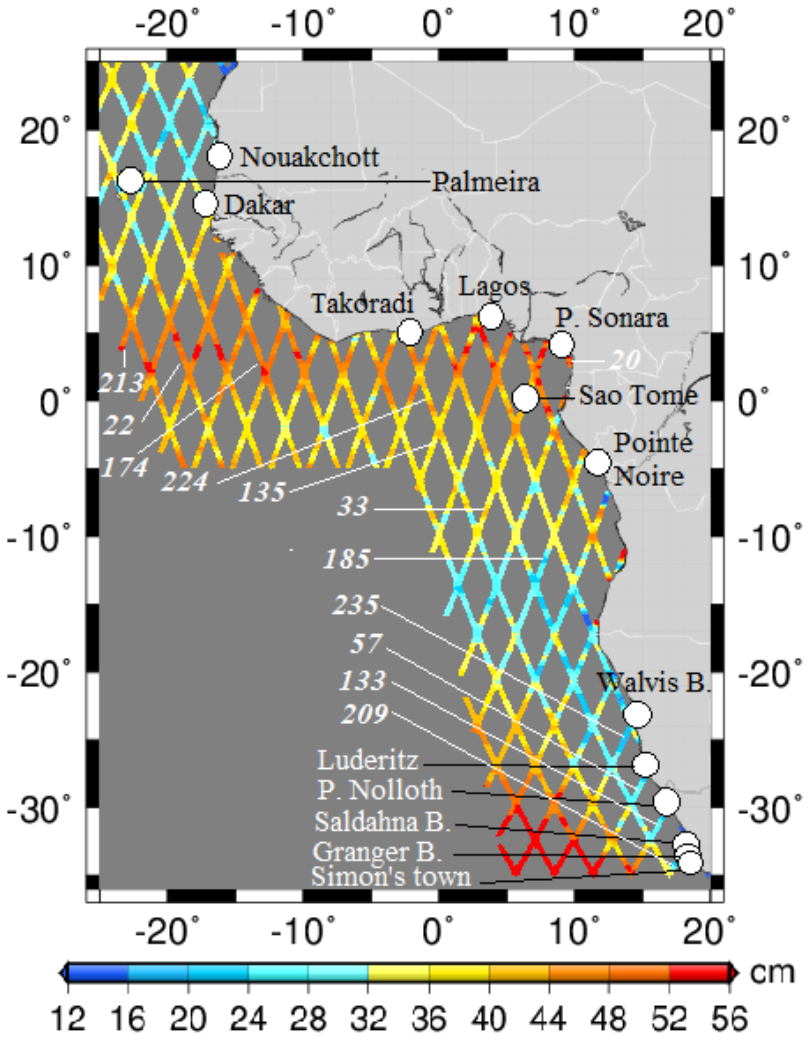

Fig.2: Taylor diagram for the SLA of X-TRACK, CMEMS/DT2014 and NEMO.1/4 compared to the TG (taken as a reference): ***(a)*** for Dakar (January 2008 – December 2014), ***(b)*** for Pointe Noire (August 2008 – June 2014) and ***(c)*** Walvis Bay (April 2008 – December 2014). The distance to the coast along of the nearest track (see the track position in Fig.1) is indicated in color. The radial distance from the origin in black is proportional to the standard deviation (normalized by the standard deviation of the TG data). The green lines centered on the reference point (the TG data, red star in the diagram) indicate the RMS error. The correlation between both fields is given by the azimuthal position in blue. The red lines delimits the area where statistical criteria for a good agreement (correlation > 0.6, normalized standard deviation between 0.7 and 1.3 and normalized RMS < 0.8) are met.

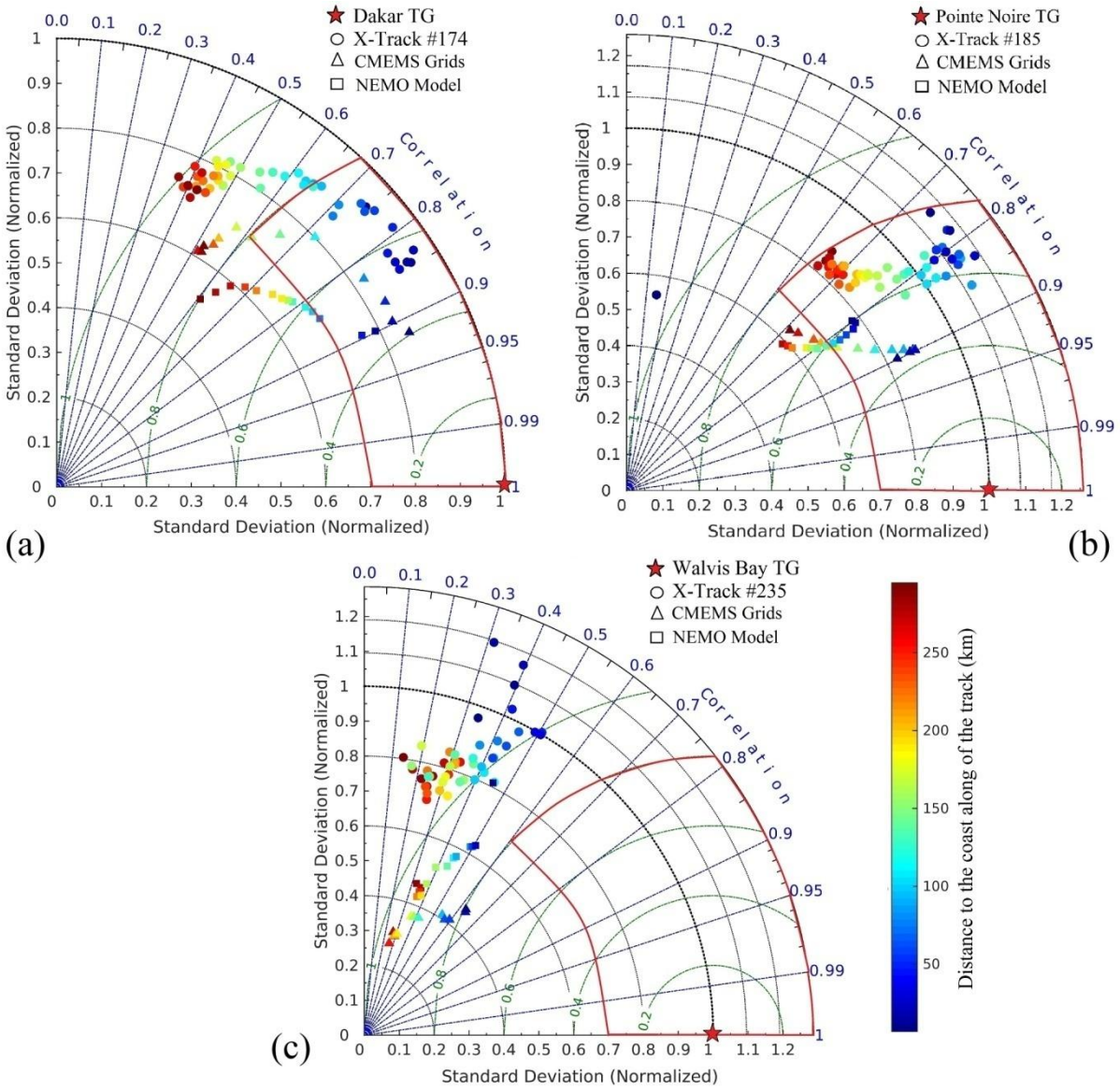

Fig.3: Maps of Correlation between TG and X-TRACK SLA (above) and RMS of the difference between TG and X-TRACK SLA (below) calculated over 2008 – 2014 period. From left to right: Dakar, Pointe Noire and Walvis Bay.

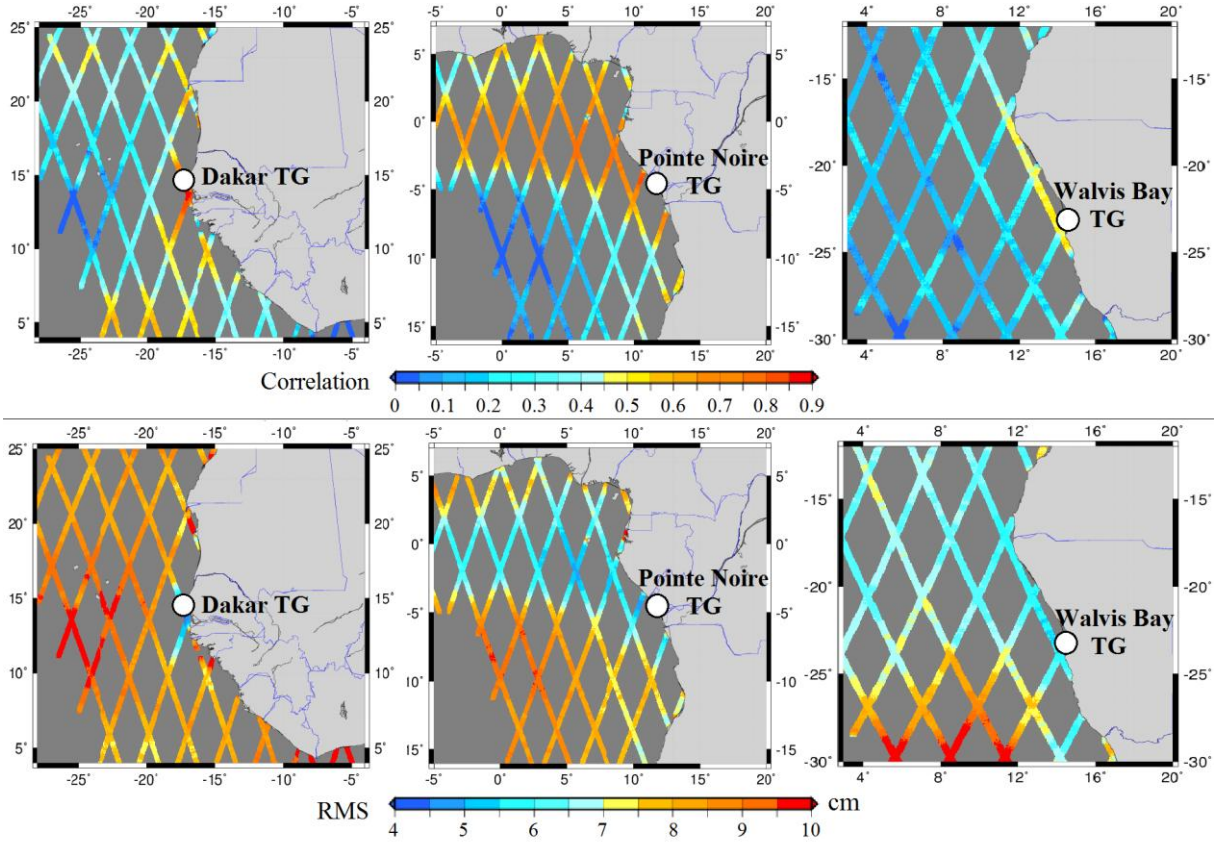

Fig.4: Maps of Correlation (above) and RMS of the difference (below) between TG and ***(a)*** CMEMS/DT2014 SLA and ***(b)*** NEMO.1/4 SLA, calculated over 2008 – 2014 period. From left to right: Dakar, Pointe Noire and Walvis Bay.

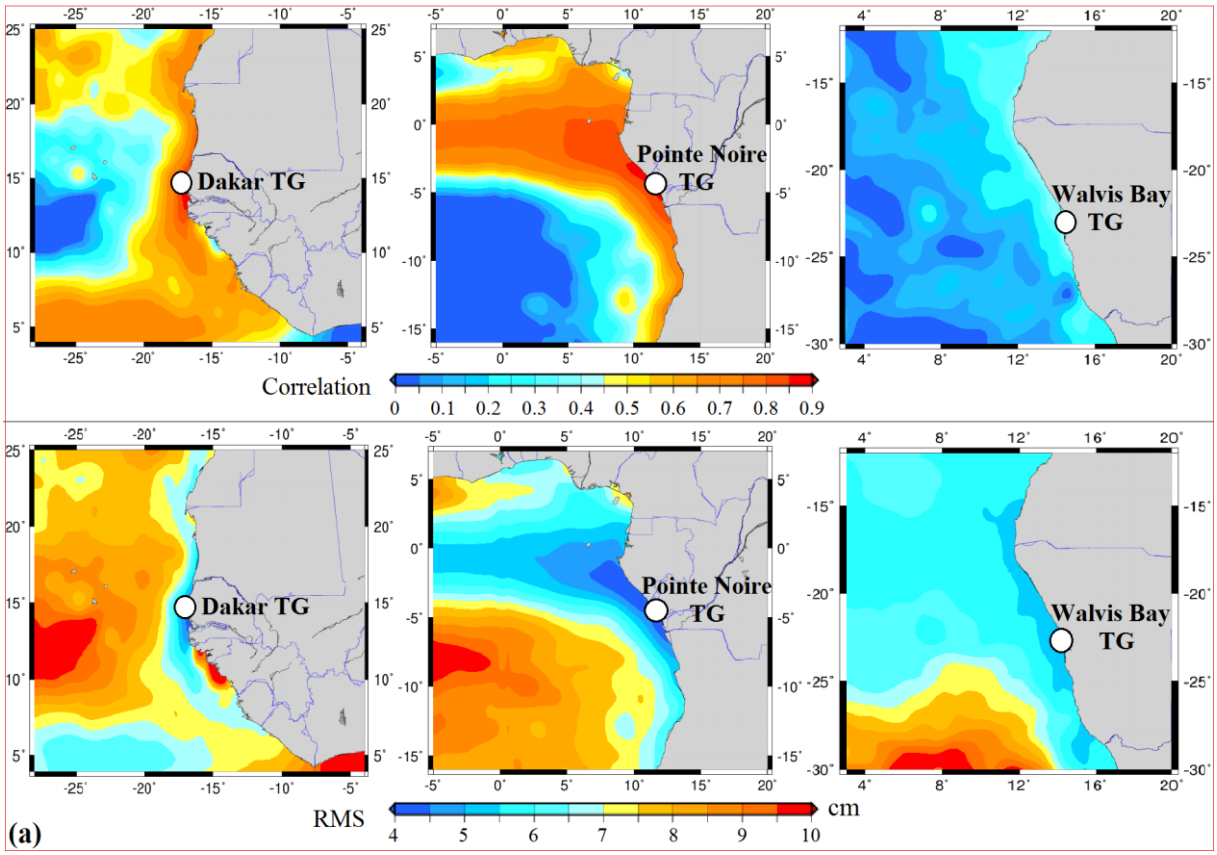
Dakar TG
Pointe Noire TG
Walvis Bay TG
Correlation
0 0.1 0.2 0.3 0.4 0.5 0.6 0.7 0.8 0.9
Dakar TG
Pointe Noire TG
Walvis Bay TG
RMS
cm
4 5 6 7 8 9 10
(a)

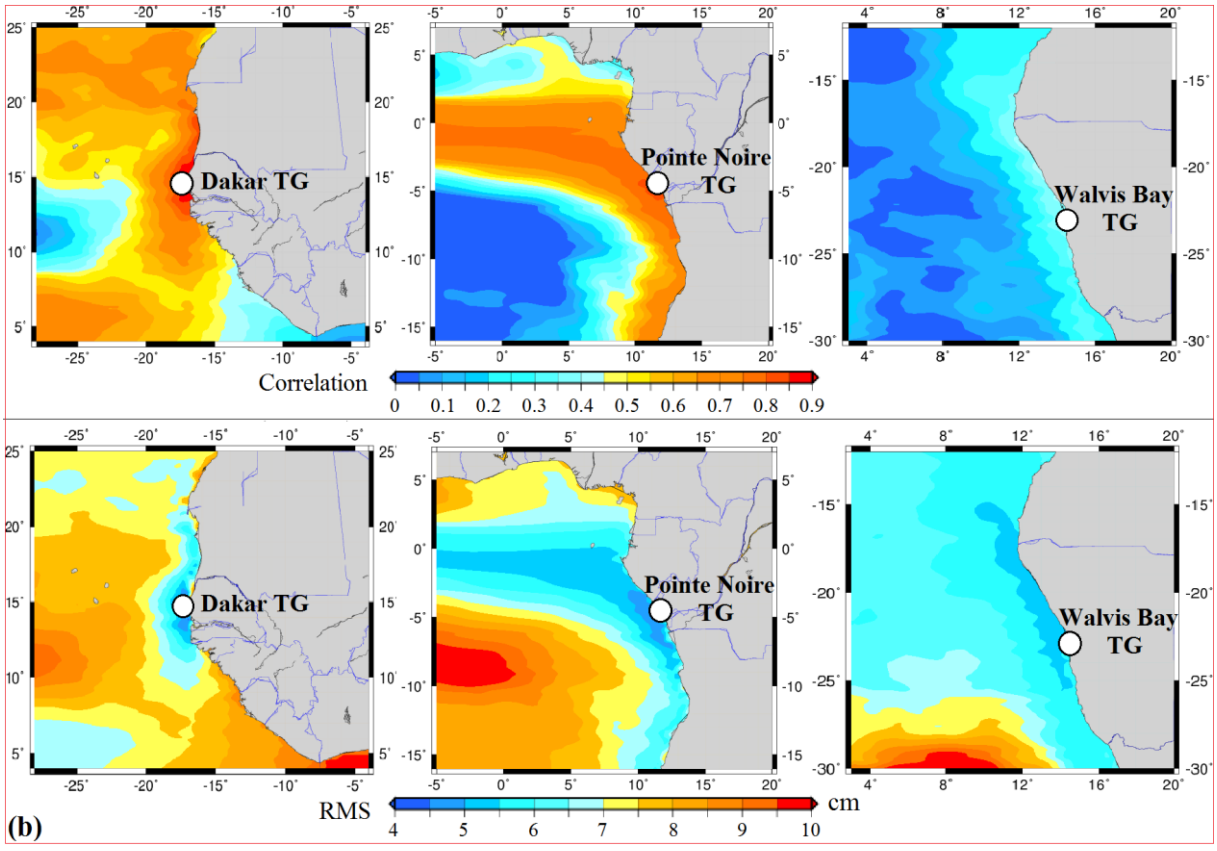
Dakar TG
Pointe Noire TG
Walvis Bay TG
Correlation
0 0.1 0.2 0.3 0.4 0.5 0.6 0.7 0.8 0.9
Dakar TG
Pointe Noire TG
Walvis Bay TG
RMS
cm
4 5 6 7 8 9 10
(b)

Fig.5: Hovmüler diagrams (distance to the coast / time) of X-TRACK SLA over 2008 – 2014 period for ***(a)*** track number 174 (Dakar area), ***(b)*** track number 185 (Pointe Noire area) and ***(c)*** track number 235 (Walvis Bay area). Units: cm.

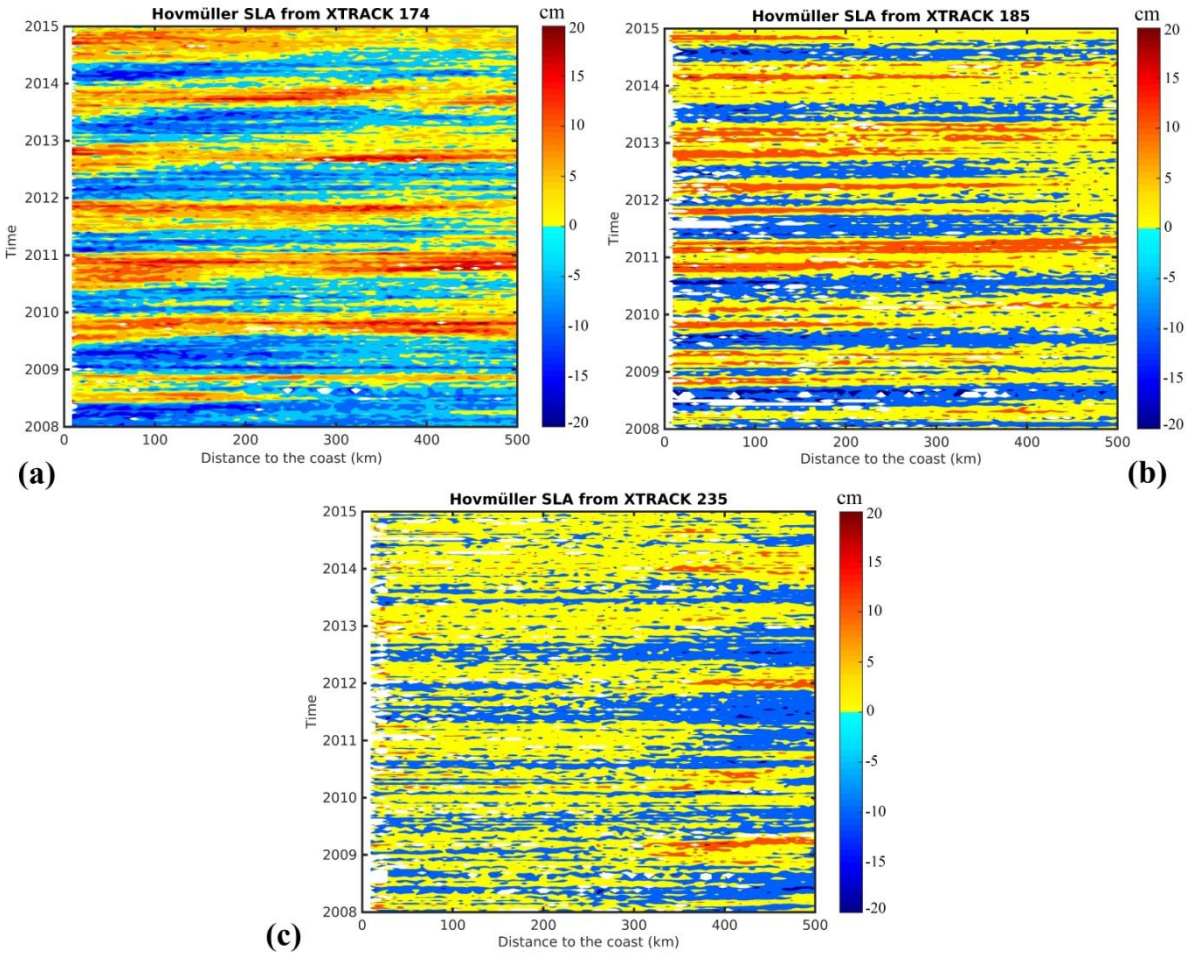

Fig.6: Comparison of SLA time-series from TG and X-TRACK, CMEMS/DT2018 and NEMO.1/12 model, for Dakar, Pointe Noire and Walvis Bay. Altimetry and model products are taken 15 km from the coast along of the altimeter track.

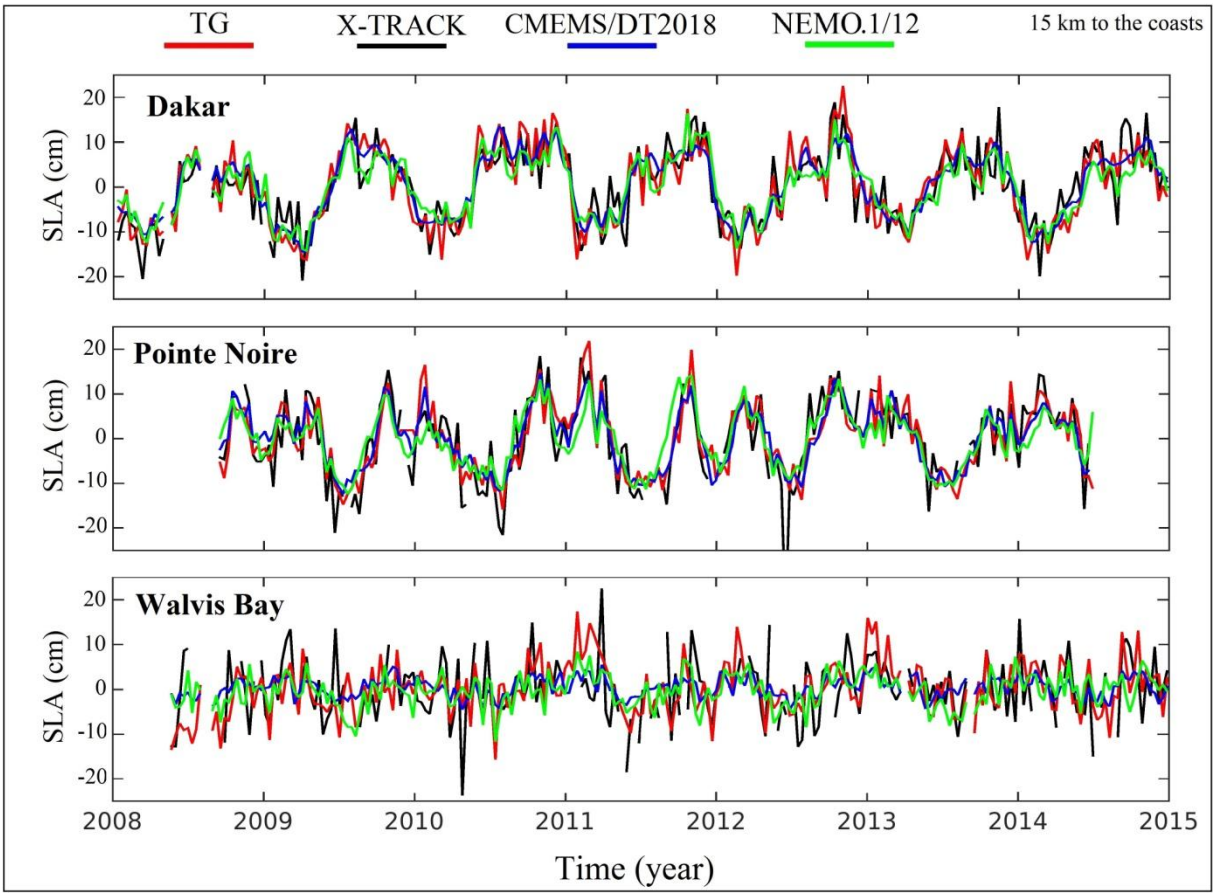

Fig.7: The amplitude and period of the FFT signal from X-TRACK (black curves), CMEMS/DT2018 (blue curves) and NEMO.1/12 model (green curves) SLA (point located 15 km from the coast) and TG SLA (red curves): above for Dakar (track 174), in the middle for Pointe Noire (track 185), below for Walvis Bay (track 235). The highest peaks of variability are indicated. Note that the scales for the FFT amplitude are different for each zone.

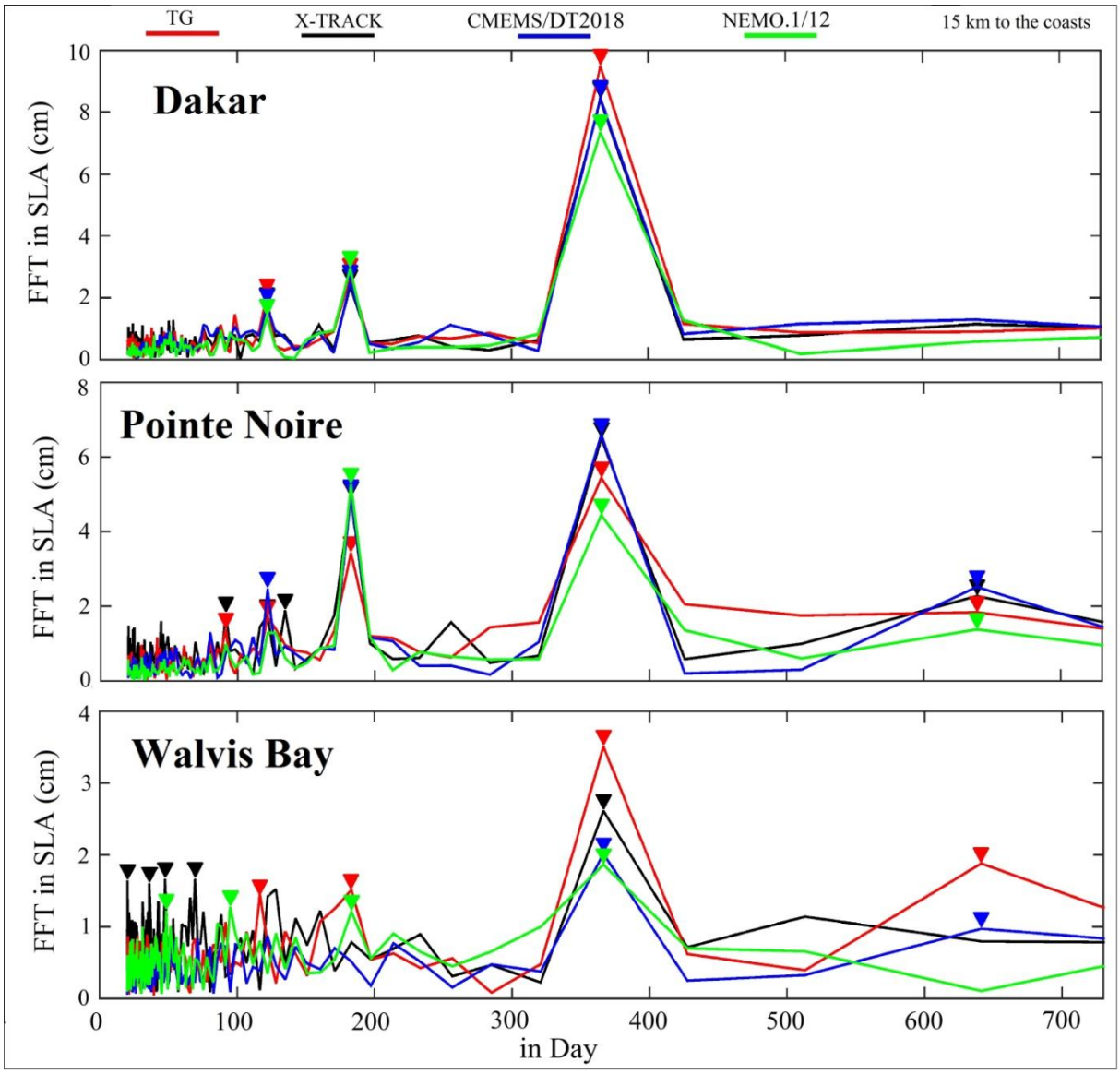

Fig.8: Maps of SLA amplitude of ***(a)*** 1st, ***(b)*** 2nd and ***(c)*** 3rd FFT maximum with the corresponding periods, below, calculated over the period 2008-2014. From left to right: X-TRACK, CMEMS/DT2018 and NEMO.1/12 model (with NEMO.1/4 above 16 °N). Note that the color scale for the period of (c) is different from those of (a) and (b), for a better visibility.

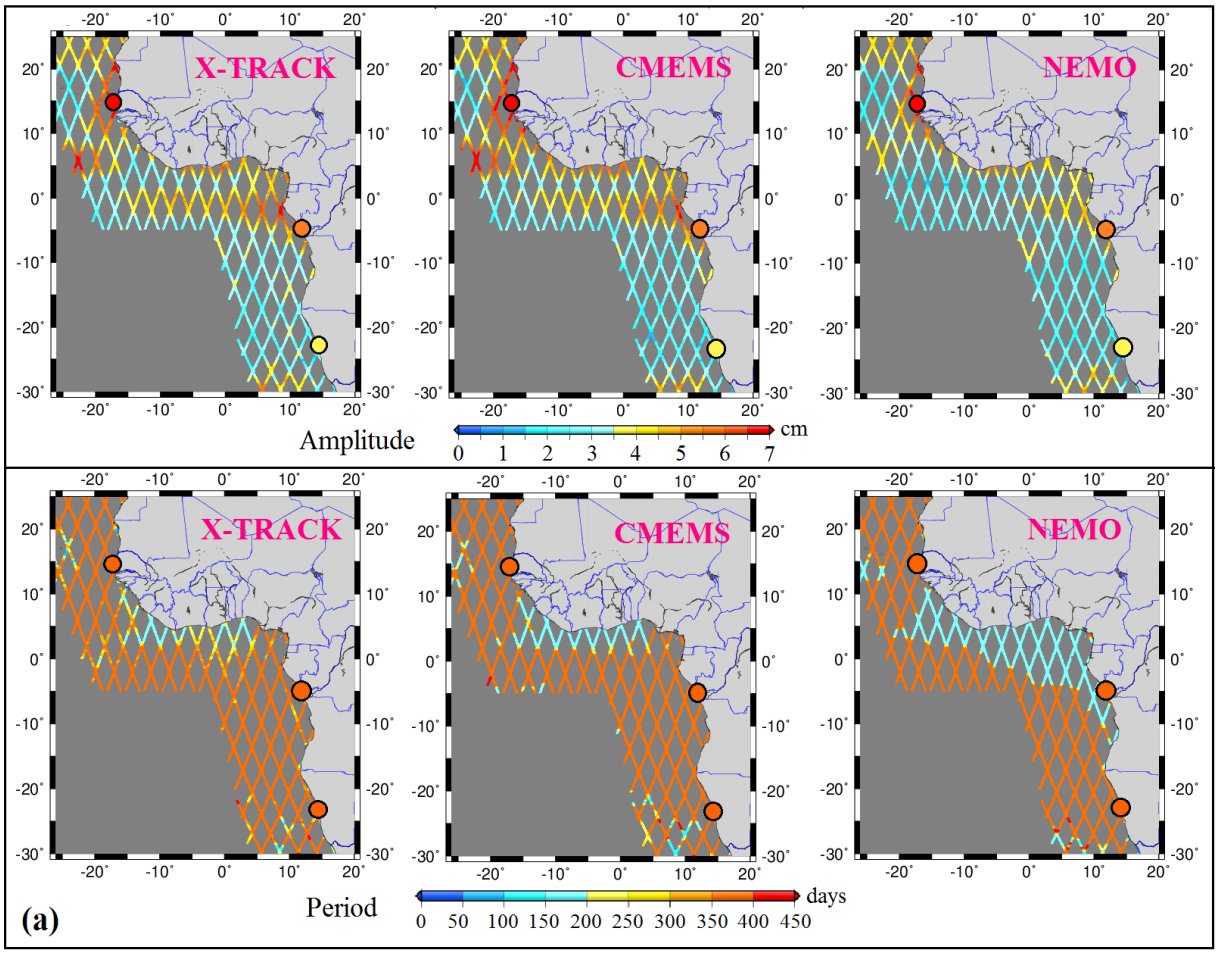

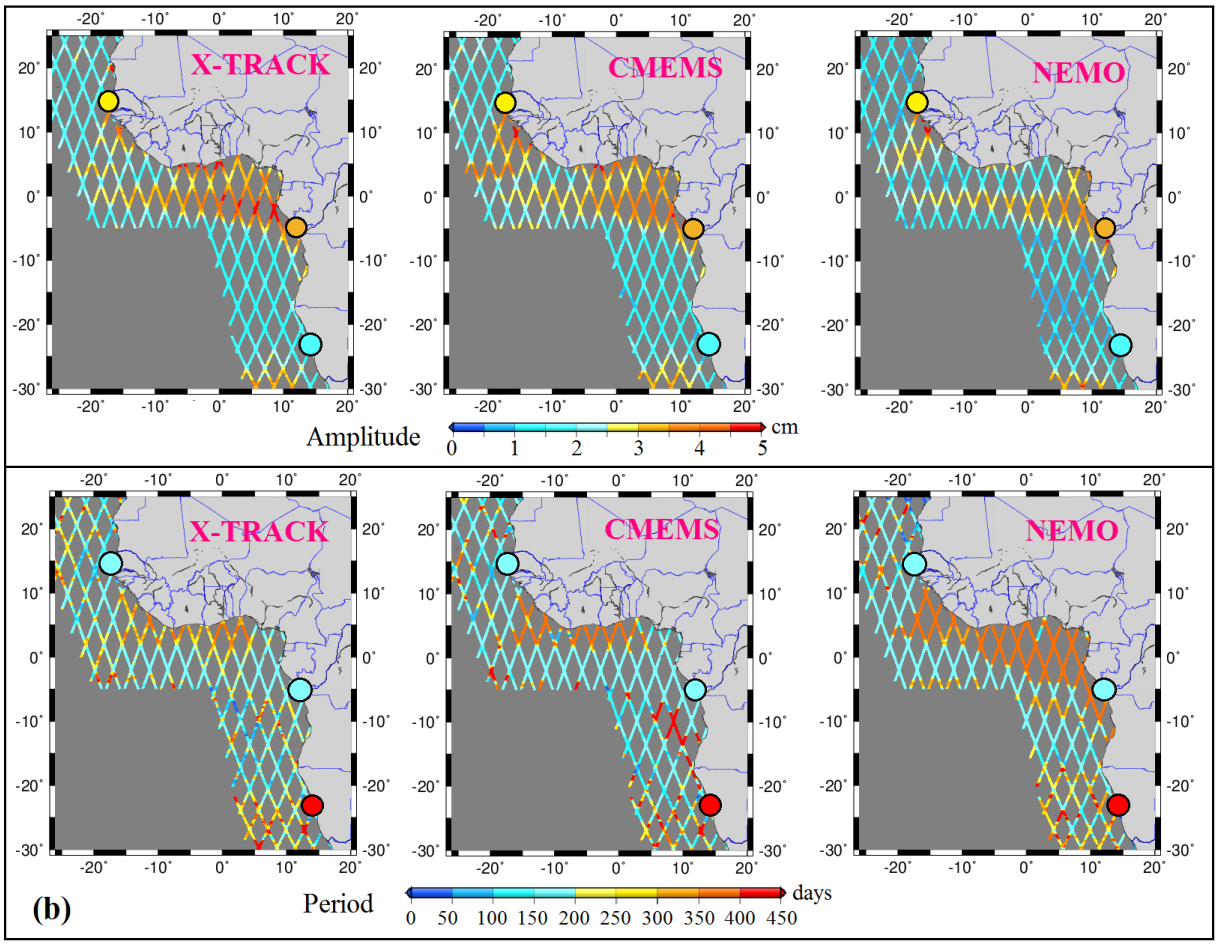
X-TRACK
CMEMS
NEMO
Amplitude
0 1 2 3 4 5
cm
X-TRACK
CMEMS
NEMO
(b)
Period
0 50 100 150 200 250 300 350 400 450
days

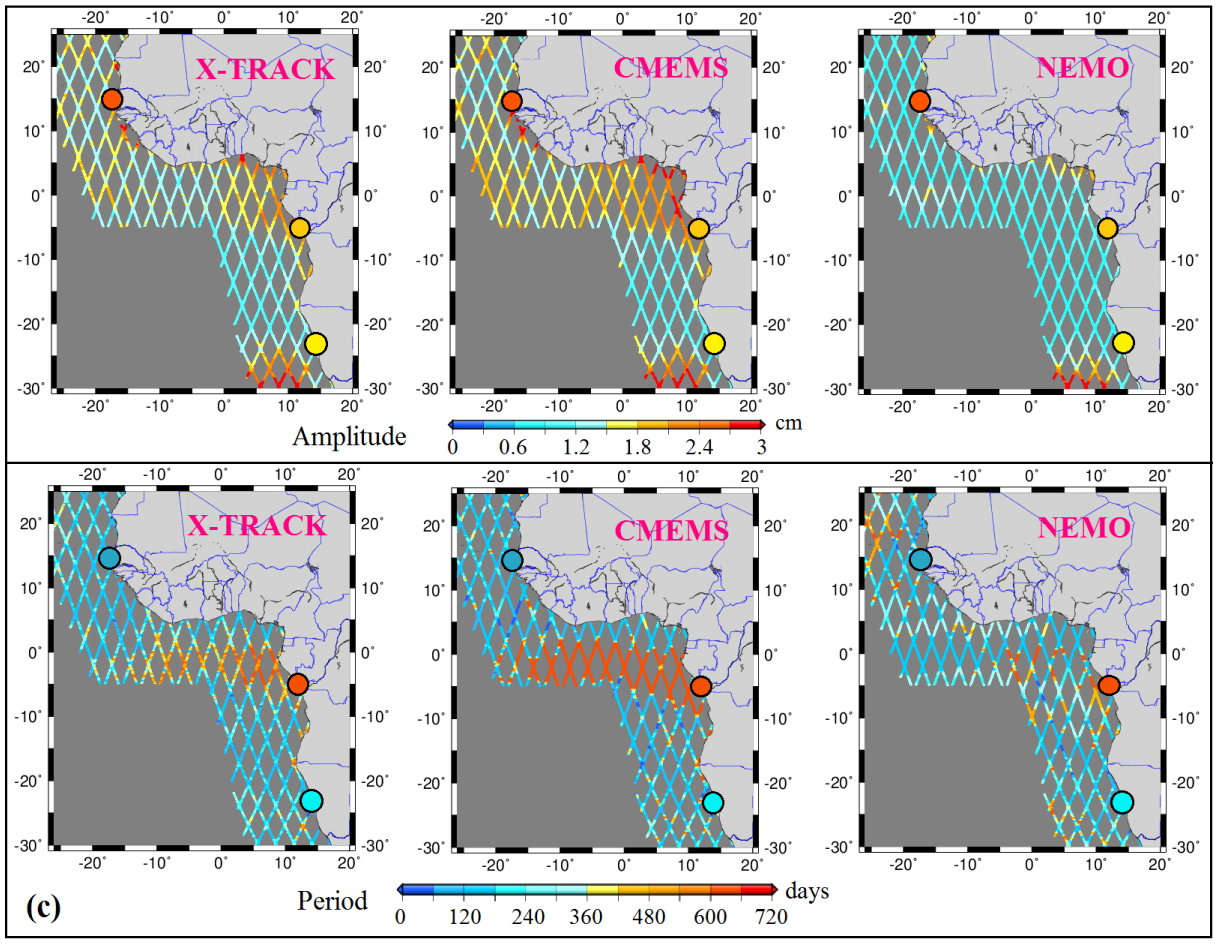
X-TRACK
CMEMS
NEMO
Amplitude
0 0.6 1.2 1.8 2.4 3
cm
X-TRACK
CMEMS
NEMO
(c)
Period
0 120 240 360 480 600 720
days